

## Late Variscan deformation events in the Bardo Syncline revealed by biotite K-Ar dating of Ludlow-age tuffite (Holy Cross Mountains, Poland)

Emil WÓJCIK<sup>1, \*</sup>, Andrzej PELC<sup>2</sup> and Adrian PACEK<sup>2</sup>

<sup>1</sup> University of Warsaw, Faculty of Geology, Żwirki i Wigury 93, 02-089 Warszawa, Poland

<sup>2</sup> Maria Curie-Skłodowska University, Institute of Physics, Plac M. Curie-Skłodowskiej 1, 20-031 Lublin, Poland

Wójcik, E., Pelc, A., Pacek, A., 2021. Late Variscan deformation events in the Bardo Syncline revealed by biotite K-Ar dating of Ludlow-age tuffite (Holy Cross Mountains, Poland). *Geological Quarterly*, 2021, 65: 15, doi: 10.7306/gq.1586

Associate Editor: Tomasz Bajda



In the Bardo Syncline (Holy Cross Mountains, Poland), two beds of tuffite (named the Niewachłów tuffites) have been discovered within greywackes of Ludlow (Silurian) age. K-Ar dating of the lower bed yielded an age of  $292.8 \pm 4.0$  Ma, while the upper bed provided an age of  $341.9 \pm 4.3$  Ma. The dates pertain to metamorphic alteration of the tuffite, related to reactivation of the Daleszyce Fault Zone. In this zone, biotite crystals present in the foliation zones were recrystallized and their K-Ar isotopic system was rejuvenated in a temperature range of  $\sim 270\text{--}300^\circ\text{C}$ . The dates that were obtained define the ages of two tectono-metamorphic episodes and reflect the timing of displacements along the fault which, in turn, reflect two deformation phases during the Variscan Orogeny (Mississippian and Early Permian). Moreover the dates may be correlated with Late Variscan magmatic activity in the Holy Cross Mountains and adjacent areas. The deformation of the Daleszyce Fault Zone may be regarded as resulting from displacements of lithospheric blocks within the Trans European Suture Zone during the Late Variscan reconstruction of the Baltica palaeocontinent margin.

Key words: Niewachłów tuffites, biotite deformation dating, illite-smectite, Ludlow, Daleszyce Fault Zone, Holy Cross Fold Belt.

### INTRODUCTION

The Holy Cross Fold Belt (HCFB) is situated in the southern part of Central Poland (Fig. 1A). In a tectonic sense, it belongs to the Trans European Suture Zone (TESZ) (Pharaoh, 1999; Winchester et al., 2002a) – a >2000 km-long tectonic zone that transects Central Europe, extending between the Black Sea and the North Sea (Pharaoh et al., 1996; Grad et al., 2002). The TESZ separates (Fig. 1A) the Precambrian East European Platform from the Paleozoic platform of Western and Central Europe (Berthelsen, 1992; Grad et al., 1999; Pharaoh et al., 2006). The TESZ consists of numerous lithospheric blocks amalgamated during the interval between the Cambrian and Carboniferous, to the SW margin of the Baltica palaeocontinent (Pharaoh, 1999; Belka et al., 2002; Winchester et al., 2002b, 2006; Nawrocki and Poprawa, 2006; Pharaoh et al., 2006) but for opposing views see Malinowski et al. (2005), Żelaźniewicz et al. (2009), Mazur et al. (2015) and Smit et al. (2016). Addi-

tionally the HCFB forms (Fig. 1A) the easternmost part of the Variscan external belt in Western and Central Europe (Aleksandrowski and Mazur, 2017; Krzywiec et al., 2017a, b; Mazur et al., 2018). The HCFB represents the only place where Paleozoic basement belonging to the TESZ can be studied at the surface. For this reason, the Paleozoic rocks of the HCFB are of great importance for understanding the Variscan tectonic evolution of the TESZ.

Recently, additional tuffite beds have been discovered in the Bardo Syncline (Fig. 1B) belonging to the HCFB (Wójcik, 2017), which occur within Upper Silurian (Ludlow) greywackes. Biotite grains separated from the tuffite were used for more precise determination of the Silurian greywacke age, using the K-Ar dating method. In this paper, an explanation is given for the discrepant age results of the K-Ar dating from these Upper Silurian tuffites.

### GEOLOGICAL SETTING

The Holy Cross Fold Belt traditionally is subdivided into two units (Czarnocki, 1919, 1957) that differ in both tectonic and stratigraphic features (Fig. 1B), i.e., the northern unit – the Łysogóry region, and the southern unit – the Kielce region. These two units are separated by a WNW–ESE striking tectonic boundary (Fig. 1B), referred to as the Holy Cross Fault. Accord-

\* Corresponding author, e-mail: [emilwojcik@student.uw.edu.pl](mailto:emilwojcik@student.uw.edu.pl)

Received: March 7, 2020; accepted: January 15, 2021; first published online: March 16, 2021

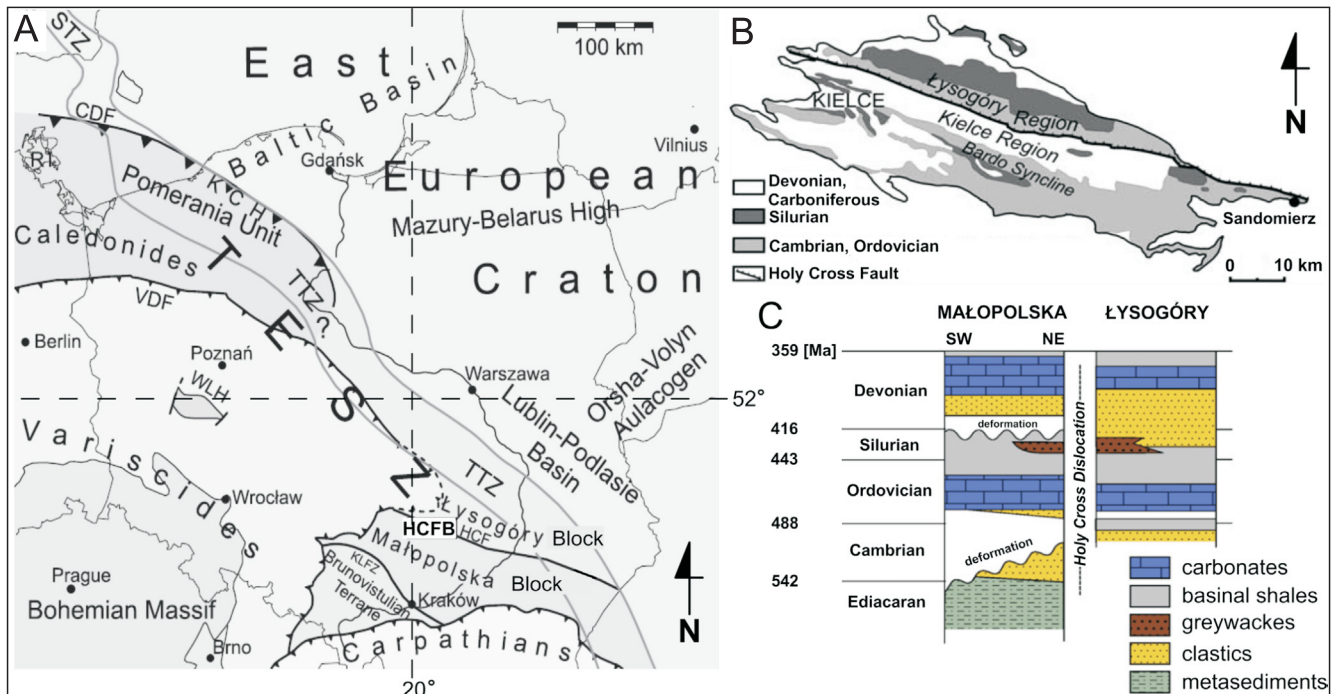


**Fig. 1A** – sketch tectonic map of Central Europe (after [Pożaryski et al., 1992](#); [Winchester et al., 2002b](#); [Mazur and Jarosiński, 2006](#); [Nawrocki and Poprawa, 2006](#); changed); CDF – Caledonian Deformation Front, HCF – Holy Cross Fault, HCFB – Holy Cross Fold Belt, KCH – Koszalin-Chojnice Zone, KLFZ – Kraków-Lubliniec Fault Zone, RI – Rügen Island, STZ – Sorgenfrei-Tornquist Zone, TESZ – Trans-European Suture Zone, TTZ – Teisseyre-Tornquist Zone, WLH – Wolsztyn-Lesznó High, VDF – Variscan Deformation Front; **B** – geological sketch map of the Holy Cross Fold Belt (after [Malec et al., 2016](#); changed); **C** – generalized stratigraphy of the Łysogóry and Małopolska regions (after [Walczak and Belka, 2017](#))

ing to [Lamarque et al. \(2003\)](#), the Holy Cross Fault initially formed in the Devonian as an oblique-slip fault under transensional conditions. It was reactivated as a reverse fault during Variscan time in a transpressional stress field. Later reactivation of the fault took place during the Alpine orogeny ([Lamarque et al., 1999](#)) when the fault returned to its oblique-slip nature. In contrast, [Gagała \(2015\)](#) interpreted the Holy Cross Fault as a thrust or reverse fault activated during both Late Caledonian and Variscan deformational episodes. Both these regions of the HCFB, separated by the fault, are part of two larger-scale tectonic units. The Łysogóry region belongs to the Łysogóry Block, while the Kielce region forms the northern part of the Małopolska Block ([Fig. 1A](#); e.g., [Pożaryski et al., 1992](#); [Dadlez et al., 1994](#); [Schätz et al., 2006](#)). The provenance of the lithospheric blocks forming the HCFB basement is still a matter of debate; however, according to most authors, the Małopolska Block represents a terrane proximal to the Baltica palaeocontinent which was initially displaced along its SW edge ([Dadlez, 2001](#); [Nawrocki et al., 2007](#)). A similar view became common in relation to the Łysogóry Block, the basement geophysical feature of which are related to the East European Platform ([Nawrocki and Poprawa, 2006](#); [Narkiewicz et al., 2015](#)).

The lithostratigraphic successions of rocks exposed in the HCFB area include rocks whose age ranges from the Cambrian to Carboniferous ([Czarnocki, 1919, 1957](#)). The successions reveal significant differences ([Czarnocki, 1936](#); [Tomczyk, 1962](#); [Kowalczewski et al., 2006](#); [Malec, 2006](#); [Trela, 2006](#); [Kozłowski et al., 2014](#)) between the Kielce region and the Łysogóry region in terms of the tectonics, stratigraphy and facies. In the Kielce region ([Fig. 1C](#)), two angular unconformities related to the Caledonian orogeny have been recorded which have no counterparts in the Łysogóry region. The first one is interpreted as Mid-

dle Cambrian ([Szczepanik et al., 2004](#); [Gagała, 2005](#)) or relating to Cambrian-Ordovician transition folding ([Samsonowicz, 1934](#)), and the second one is referred to Late Caledonian folding ([Fig. 1C](#)) which occurred between the Late Silurian and the Early Devonian ([Kowalczewski and Lisik, 1974](#); [Malec, 2001](#)). It was only the succeeding Variscan Orogeny that was marked in both HCFB regions by folding, with an ensuing distinctive angular unconformity and stratigraphic gap between the Mississippian (Visean) and the Upper Permian rocks ([Kowalczewski and Rup, 1989](#); [Szulczewski, 1995](#); [Lamarque et al., 2003](#)). Palaeomagnetic data obtained from Devonian carbonate rocks suggest that Variscan orogeny involved two stages: the first stage took place during the Visean and the second one occurred in the Early Permian ([Grabowski et al., 2006, 2009](#); [Szaniawski, 2008](#)). The tectonic deformation episodes within the HCFB were accompanied by magmatic and hydrothermal activity related to minor intrusions of diabase and lamprophyre ([Czarnocki, 1919](#); [Kardymowicz, 1957, 1962](#); [Rubinowski, 1962](#); [Nawrocki, 2000](#); [Krzemińska and Krzemiński, 2019](#)). Although the age of magmatism is controversial, several phases of their activity increase have been identified. The first of these, the late Caledonian stage, occurred close to the Silurian/Devonian boundary ([Nawrocki et al., 2013](#)), and a following phase took place in the Mississippian (Serpukhovian) ([Nawrocki et al., 2013](#); [Krzemińska and Krzemiński, 2019](#)). The final stage of magmatic activity in the HCFB occurred during the Middle Triassic ([Nawrocki et al., 2013](#)).

Along the southern part of the Kielce region, the Chęciny-Klimontów Anticlinorium extends in a WNW–ESE direction ([Kowalczewski and Rubinowski, 1962](#); [Orłowski and Mizerski, 1995](#); [Konon, 2008](#)). The axial part of this anticlinorium ([Walczowski, 1968](#); [Filonowicz, 1976](#)) contains the Bardo

Syncline (Fig. 1B). Within the Ludlow deposits of the Bardo Syncline, two beds of tuffite (named the Niewachłów tuffites) were found, the object of the study described in this work. The Bardo Syncline basement is composed of Lower and Middle Cambrian siliciclastic rocks (Fig. 2; Mizerski et al., 1986; Orłowski and Mizerski, 1995; Kowalczewski et al., 2006), which are overlain by Ordovician strata with an angular unconformity reaching  $>60^\circ$  (Czarnocki, 1928). The Ordovician rocks show considerable lithological diversity (Fig. 2; Tomczyk, 1962; Bednarczyk et al., 1966; Trela, 2006). The Silurian strata begin with graptolite shales, which in the upper part of the succession (Upper Ludlow) are gradually succeeded (Fig. 2) by greywackes included in the Niewachłów Beds (Czarnocki, 1919; Stupnicka, 1995; Malec, 2001; Masiak, 2007, 2010). At the boundary of the graptolite shales and the greywacke occurs a sill-type magmatic intrusion which is traditionally referred to as the Bardo Diabase (Czarnocki, 1919, 1939). The geochemical composition of the intrusion corresponds to tholeiitic basalt

(Krzemiński, 2004). The diabase intruded into flat-lying Silurian rocks and was then folded together with them into a syncline between the Late Silurian and the Early Devonian (Kowalczewski and Lisik, 1974). Such a succession of events is indicated by the pre-folding nature of the magnetic primary natural remnant magnetization of the diabase noted by Nawrocki (1999). Moreover, geochemical signatures implying an extensional tectonic setting during magma emplacement (Krzemiński, 2004), along with Ar-Ar dates of  $412 \pm 2$  Ma and  $415 \pm 2$  Ma (Nawrocki et al., 2013), are consistent with the Ludlow age of the diabase.

Above the Niewachłów greywackes, a stratigraphic gap extends from the Upper Silurian to the Lower Devonian (Czarnocki, 1936; Malec, 2001; Kozłowski et al., 2014; Malec et al., 2016). Emsian siliciclastic rocks and Eifelian dolomites lie unconformably on the older rocks (Fig. 2; Czarnocki, 1919; Racki, 2006) and were folded during the Variscan orogeny together with the Lower Paleozoic basement (e.g., Szulczewski, 1995; Lamarche et al., 2003 and references cited therein).

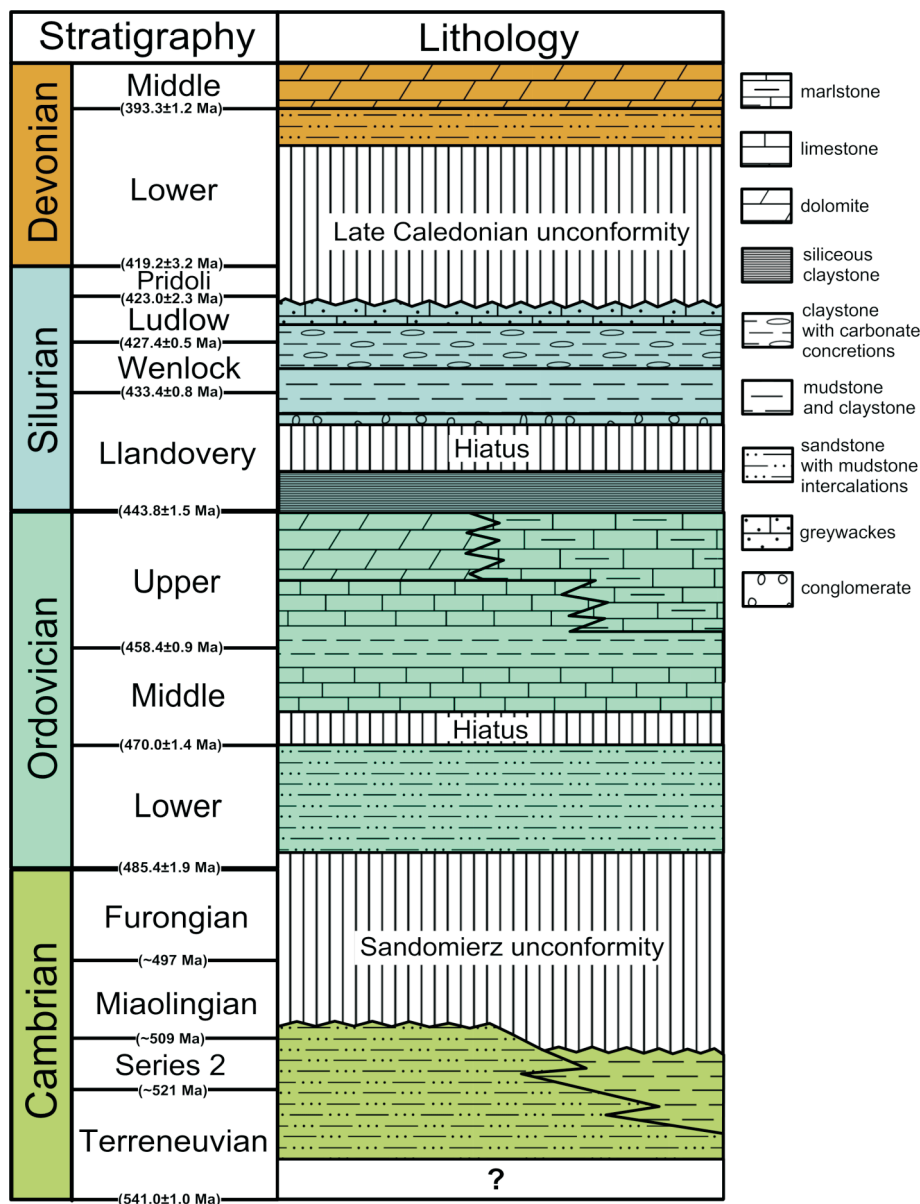


Fig. 2. Lithostratigraphy of the Lower Paleozoic rocks exposed in the Bardo Syncline (after Tomczyk, 1962; Kowalczewski et al., 2006; Trela, 2006; Malec, 2006; Racki, 2006; Żylińska, 2017)

## POSITION OF THE TUFFITE BEDS IN THE LUDLOVIAN STRATIGRAPHIC PROFILE

In the area where rocks of the southern limb of the Bardo Syncline are exposed, an exposure of Upper Silurian rocks (Upper Ludlow) is present (Fig. 3A, B). In an undercut slope bank, greywackes of the Niewachłów Beds occur, components of which include fine, medium and coarse sandstones, siltstones and mudstones. The exposure is intersected by a fault zone (Fig. 3A, B) accompanied by intense deformation. The western part of the exposure chiefly comprises coarse-grained greywackes (Fig. 4A), whereas the eastern part contains mostly siltstone and claystone. In the eastern part of the exposure, two previously unknown tuffite beds were discovered (Fig. 4B–D). Several minor lenses containing pyroclastic material are also visible in the succession (Fig. 4B). The tuffite beds are intersected by shear zones accompanied by cataclasite (Figs. 4A and 5A). The tuffite occurs within greywacke (siltstone, claystone and siliceous shale; Fig. 4B). The average orientation of the beds is 42/55 and flat parallel lamination can be observed internally. The vertical distance between the lower tuffite and the upper tuffite reaches 80 cm. The thickness of the tuffite beds ranges between 30 and 40 cm. The tuffite is yellowish and contains local light grey patches (Fig. 4C, D). It is composed of fine and medium grained clastic material containing mainly quartz, biotite, sparse feldspar grains and a matrix of clay minerals. Individual constituents do not reveal signs of advanced weathering. Examination with the naked eye revealed lamination resulting from a flat parallel arrangement of the biotite and quartz grains which generally follows the bedding. In the upper tuffite, the lamination is slightly disturbed.

## DALESZYCE FAULT ZONE (DFZ)

The Bardo Syncline is bounded by faults to the north and the south (Fig. 3A, B). To the north is the Góra Ryj Fault (Czarnocki, 1919; Kowalczewski and Lisik, 1974) while to the south there is a fault that may be correlated with the Daleszyce Fault Zone (Filonowicz, 1976; Konon, 2007). In the vicinity of the exposure, the DFZ is a minimum 150 m-wide strike-slip fault zone oriented at 33/60 (Fig. 4A) which extends parallel to the Bardo Syncline (Fig. 3A, B). The orientation of this zone is similar or identical to the greywacke beds' attitude (Fig. 5C) in the southern limb of the Bardo Syncline. As a result of this "convergence", there are frequent tectonic displacements on the bed surfaces of sandstone, siltstone and greywacke-claystone beds (Fig. 5D), as well as on the tuffites (Fig. 5A). At the contacts of competent and incompetent layers (e.g., sandstone and claystone), tectonic breccias and cataclasites are present. On the fault planes, horizontal striations and minor tectonic sheets (Fig. 5B), developed along the strike, indicate dextral movement which corresponds to the displacements observed along the entire strike of the DFZ (Konon, 2007). The tectonic activity of the DFZ is responsible for the formation of numerous deformation structures in the tuffites studied.

## METHODOLOGY

Tuffite samples were taken from both beds and were cut parallel to the lineation and perpendicular to the foliation. Subsequently, thin-sections were prepared to examine microstructures

using a polarized light microscope. Point counts were made on the thin-sections in order to determine the modal compositions of the tuffites. Scanning electron microscopy (SEM) imaging using backscattered electrons and energy-dispersive spectroscopy (EDS) chemical microanalysis (*Sigma VP, Carl Zeiss Microscope GmbH*, Oberkochen, Germany) was carried out on polished thin-sections. The analyses were performed in the Cryo-SEM Laboratory, Faculty of Geology, University of Warsaw in Poland.

A preliminary description of the composition of the clastic material in a washed sample was made using a binocular microscope.

X-ray analysis (XRD) of clay minerals for both tuffite samples, one for each layer, was performed at the Clay Minerals Laboratory (ClayLab) of the Institute of Geological Sciences (Polish Academy of Sciences) in Kraków. The whole-rock samples were gently crushed and disaggregated in deionised water using an ultrasonic bath. The <2 µm size fraction was separated by sedimentation in distilled water and repeated centrifugation and dialysis. The XRD patterns of clay minerals were determined on oriented air-dried and ethylene-glycolated specimens on an XRD diffractometer *Thermo ARL X'Tra* equipped with a semiconductor detector cooled by Peltier cells, using Cu-Kα radiation a 5–65° 2θ range, a 0.02° 2θ step size and a 5s per step count time. The quantitative analysis of smectite in illite-smectite was determined by whole-pattern fitting between the calculated and the experimental intensities using the *Sybillia* program (*Chevron* proprietary software). Additionally, routine XRD investigations of the powdered whole rocks (for both tuffites) were also performed.

A binocular microscope and a microdissection needle were used to isolate biotite flakes for the isotopic age analysis. In order to remove clay minerals, each tuffite sample was rinsed 60 times in water. The magnetic fraction (including biotite) was separated with a neodymium magnet. From the rest of the magnetic fraction, biotite crystals were separated by hand under a binocular microscope. The biotite crystals used for the laboratory procedure ranged 200–500 µm in diameter and up to 150 µm in thickness. Only automorphic, unaltered biotite crystals, without any visible signs of kaolinitization, were selected for analysis. The biotite samples separated for K-Ar dating were rinsed three times in acetone. One biotite sample with a weight of 100 mg was separated from each tuffite layer.

K-Ar isotope dating was carried out at the Mass Spectrometry Laboratory, Institute of Physics, Lublin University. Concentrations of the radioactive potassium isotope <sup>40</sup>K and the stable argon isotope <sup>40</sup>Ar were determined.

The concentration of isotope <sup>40</sup>K can be calculated from the total concentration of potassium in the sample [<sup>40</sup>K concentration is 0.01167% – International Atomic Energy Agency (IAEA) data]. The total concentration of potassium was determined using the isotope dilution method. In this method, potassium is considered as a mixture of two isotopes <sup>39</sup>K and <sup>41</sup>K. The elemental analysis is hence reduced to the isotope ratio analysis of a mixture containing an investigated sample and a spike (strongly enriched in <sup>41</sup>K isotope KCl solution). The mixture of sample and spike was then completely dissolved in pure phosphoric acid (H<sub>3</sub>PO<sub>4</sub>) on a stove and dehydrated to achieve potassium phosphate (K<sub>3</sub>PO<sub>4</sub>) with a slight excess of H<sub>3</sub>PO<sub>4</sub>. Such prepared sample material was loaded onto the evaporator filament of the ion source of the Thermal Ionization *Mass Spectrometry* (TIMS) mass spectrometer. The isotope ratio of potassium  $R = {}^{39}\text{K} / {}^{41}\text{K}$  is determined by measurement of the respective ion current intensities by ion detector. The total molar con-

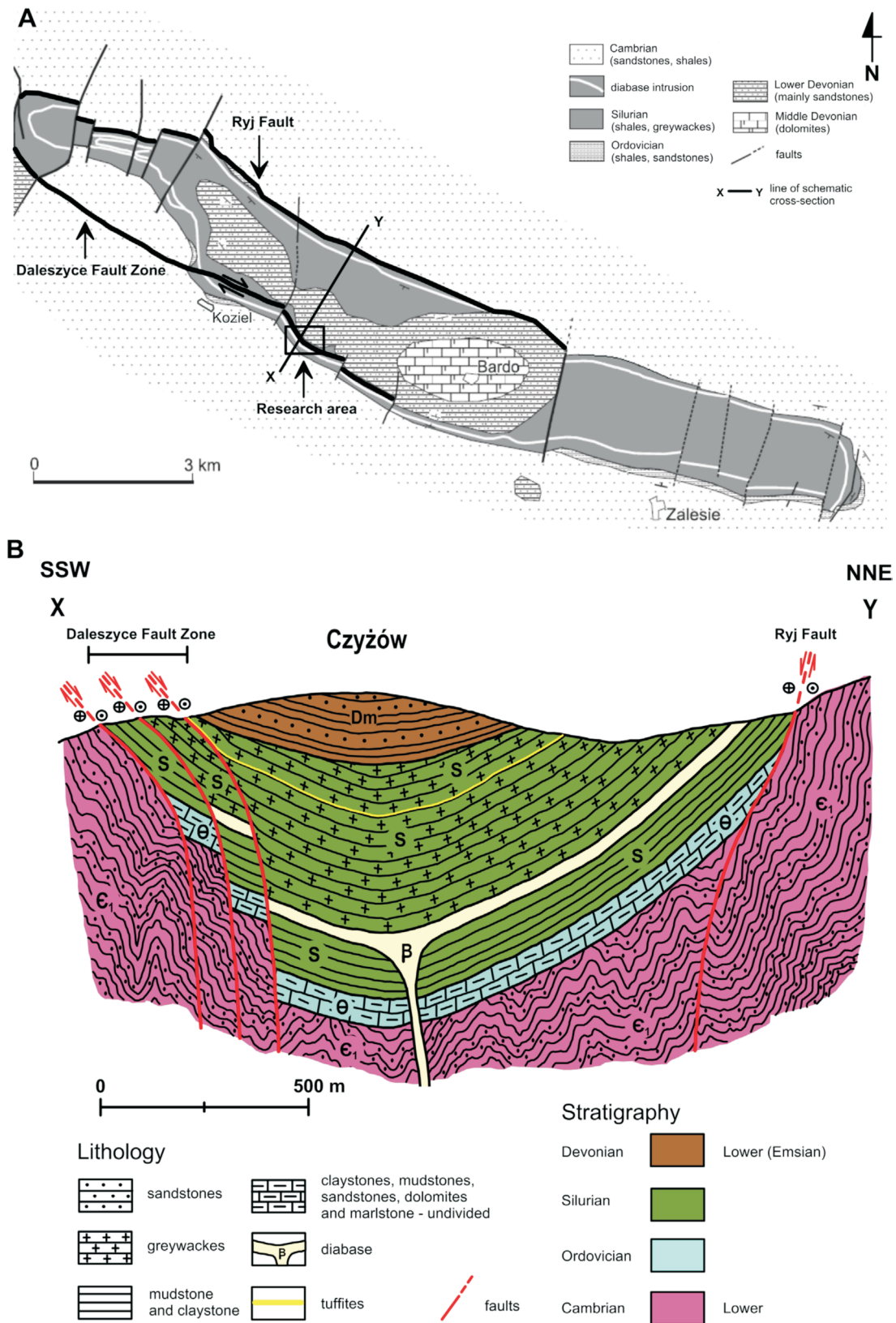
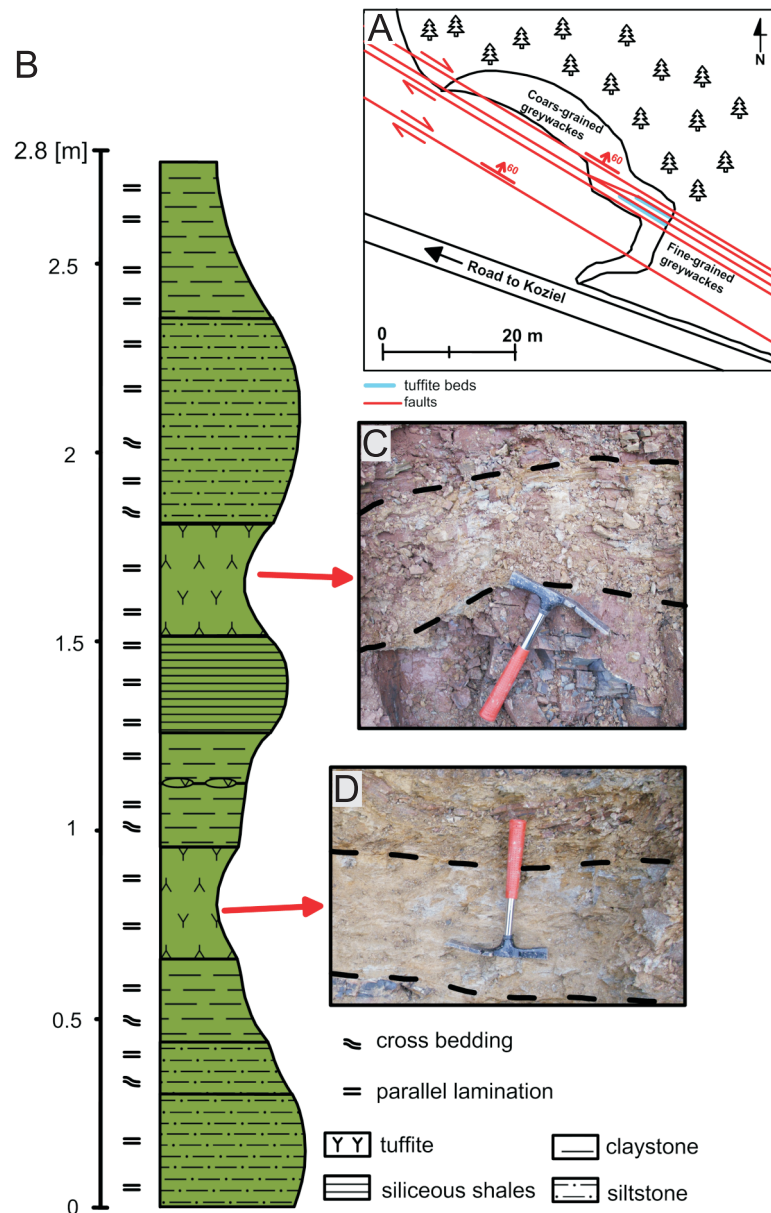


Fig. 3A – sketch geological map of the Bardo Syncline (after Czarnocki, 1958; Nawrocki and Poprawa, 2006 modified and completed with the Daleszyce Fault Zone and the Ryj Fault; B – geological cross-section through the Bardo Syncline



**Fig. 4A** – sketch map of the exposure with tuffite beds in Czyżów village; **B** – lithology of the Silurian greywackes with tuffite beds; eastern part of the exposure (see Fig. 3A for location); **C** – upper tuffite bed; **D** – lower tuffite bed

centration of potassium in the sample investigated ( $\% K_{\text{sample}}$ ) may be calculated by the following formula:

$$\%K_{\text{sample}} = \frac{m_{\text{spike}}}{m_{\text{sample}}} \cdot \frac{R_{\text{spike}} - R_{\text{mix}}}{R_{\text{mix}} - R_{\text{sample}}} \cdot \frac{1 + R_{\text{sample}}}{1 + R_{\text{spike}}} \cdot \%K_{\text{spike}}$$

where:  $m_{\text{spike}}$  is the mass of the spike,  $m_{\text{sample}}$  is the mass of the sample investigated,  $R_{\text{spike}}$  is the isotope ratio of the spike,  $R_{\text{mix}}$  is the isotope ratio of the mixture,  $R_{\text{sample}}$  is the isotope ratio of the sample investigated, and  $\%K_{\text{spike}}$  is the molar concentration of potassium in the spike.

Argon content was determined using a static-vacuum MS-10 mass spectrometer and the isotopic dilution method of the argon extracted with the rare isotope,  $^{38}\text{Ar}$  (spike). A full de-

scription of the method can be found in Halas (1995). Aliquots of samples were wrapped in aluminium foil and loaded into the extraction-purification line. In this line the samples were melted in a double-vacuum crucible and spiked with pure  $^{38}\text{Ar}$  (Institute for Inorganic and Physical Chemistry, University of Bern). Gases released from a sample were purified from non-noble gases by use of a getter pump. Using a mass spectrometer the ion beam intensities of  $^{40}\text{Ar}$ ,  $^{38}\text{Ar}$  and  $^{36}\text{Ar}$  were measured. The content of atmospheric  $^{40}\text{Ar}$  was determined by measurement of the  $^{36}\text{Ar}$  peak in the mass spectrum. To calibrate the amount of  $^{38}\text{Ar}$  spike, interlaboratory standards such as MMhb-1 (Samson and Alexander, 1987) and GLO (Odin et al., 1982) were used. The accuracy of the concentration of potassium  $^{40}\text{K}$  and  $^{40}\text{Ar}$  obtained by the isotope dilution method is better than 1%. The overall standard uncertainty (given in  $2\sigma$ ) was calculated following Cox and Dalrymple (1967).

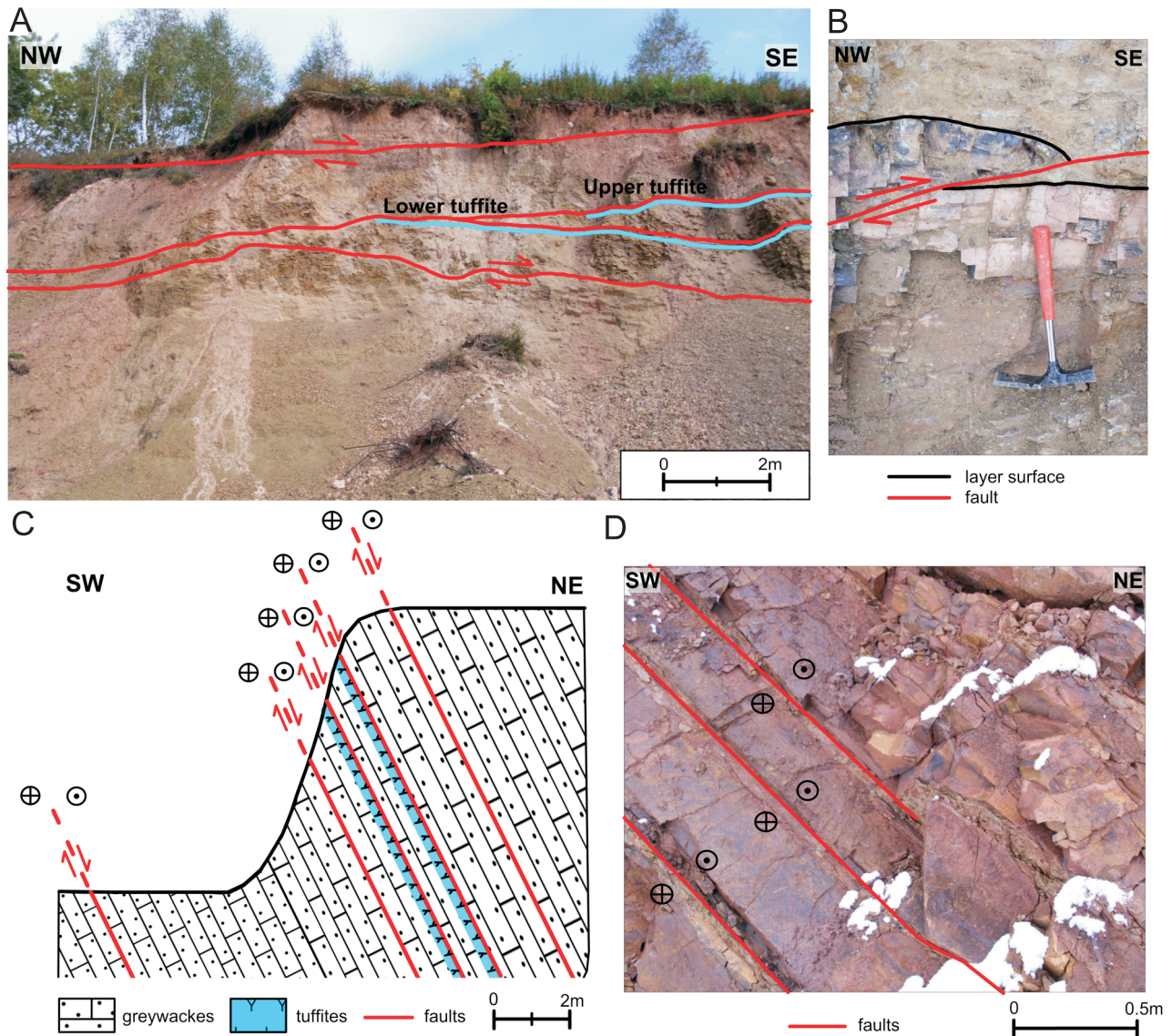


Fig. 5A – Silurian greywackes with the tuffite beds representing part of the Daleszyce Fault Zone, with a dextral shear sense; B – tectonic sheet in the greywacke strata in the exposure; C – schematic geological cross-section through the exposure showing the parallel position of faults with respect to the greywacke strata; D – photograph showing faults parallel to the greywacke strata

## RESULTS

### PETROGRAPHY OF THE NIEWACHLÓW TUFFITES

The main constituent of the mineral skeleton in the lower tuffite comprises quartz grains (>30% of the rock volume; Fig. 6A). The grains have a strongly elongated habit, and a minority contain corrosive embayments that indicate a volcanic origin, while other groups of quartz grains contain fluid inclusions (Fig. 6D). Scarce crystals with an euhedral habit were probably subjected to recrystallization. The second most important constituent is biotite, the quantity of which reaches up to 25% by volume (Fig. 6A). The crystals underwent a process of minor kaolinization (Fig. 6C) and rarely contain acicular quartz inclusions (Fig. 6H). Potassic feldspars are present in a smaller amount of <10% (Fig. 6B). Accessory minerals include crystals of garnet with biotite inclusions; zircon, which occurs mainly as inclusions

in biotite crystals (Fig. 6E); as well as apatite, barite, tridymite and chalcedony. In thin-section, altered grains of magmatic rocks are present (chiefly dacite; Fig. 6F) and lesser amounts of altered volcanic glass are visible in quantities that do not exceed 10% (Fig. 6G). In addition, sparse grains of sedimentary rocks (sandstone and siltstone) are present (Fig. 6H), which make up nearly 5% of the composition. All of these components are hosted in a matrix which constitutes ~20% of the rock (Fig. 6A) and is composed of clay minerals.

The upper tuffite in the profile differs from the lower tuffite mostly with regard to the amount of argillaceous matrix, the content of which may reach 60%. The content of biotite crystals is similar to their concentration in the lower tuffite and amounts to ~25%, their state of preservation is, however, slightly worse and the grains bear traces of more advanced kaolinization. All of the remaining constituents of the mineral skeleton occur in a proportionally smaller amount and their overall concentration

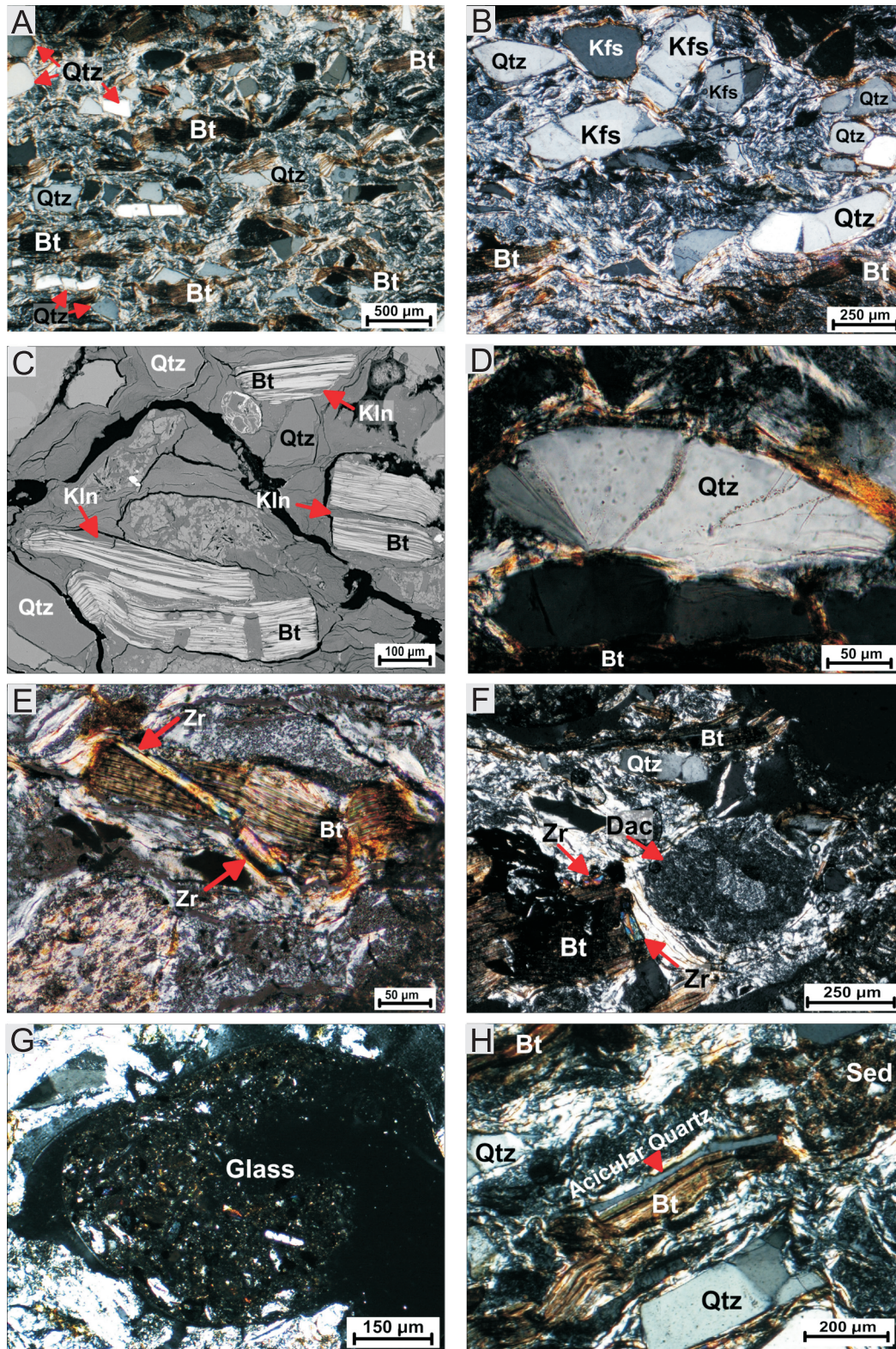


**Fig. 6.** Thin-section microphotographs of the mineral assemblages, textures and fabrics in the tuffite in cross-polarized light (except for microphotograph C)

**A** – general view showing the proportion of the main mineral components (biotite and quartz) in the lower tuffite; domino boudins in a quartz grain – bottom left corner of the photo; **B** – cracked K-feldspars and quartz grains in the lower tuffite; **C** – backscatter SEM image showing biotite crystals with kaolinite intergrowths; **D** – fluid inclusions in quartz and signs of crack healing; **E** – cracked zircon crystal in a tectonically deformed biotite flake (upper tuffite); **F** – dacite grain and biotite flake with several zircon crystals (lower tuffite); **G** – altered volcanic glass with crystals of plagioclase, amphibole and pyroxene; **H** – grain of sedimentary rock and acicular quartz in biotite flake recrystallizing as a pseudomorph after kaolinite (upper tuffite); Bt – biotite, Dac – dacite, Fsp – feldspar, Kfs – k-feldspar, Kln – kaolinite, Qtz – quartz, Sed – sedimentary grain, Zr – zircon

amounts to ~15% of the rock volume. There is an almost complete absence of feldspars.

In both of the tuffites, the presence of volcanic quartz with corrosion embayments and of clasts of volcanic rock, mainly dacite (Fig. 6F), points to a high-silica dacitic composition of the magma from which the tuffites originated. The high silica concentration of the magma is indicated not only by the quartz grains, but also by the abundant zircon crystals (Fig. 6E, F) present predominantly as inclusions in biotite grains. The occurrence of zircon grains in biotite and their high concentration (several crystals in a biotite aggregate) cannot result from metamorphic alteration but points to a volcanic origin. In addition, clasts of K-feldspar were observed in the tuffite (Fig. 6B), the presence of which indicates a high potassium concentration in the parent magma of the tuffites. In summary, the tuffite source-area volcanism probably had the nature of a high-potassic dacite with a relatively large silica concentration.

#### DEFORMATION STRUCTURES IN THE TUFFITES

Investigations of thin-sections confirmed the presence of deformation structures previously observed at exposure, and these occur both in individual grains and in packages.

The quartz, which makes up the largest part of the tuffites, usually has an elongated habit (Fig. 6A) and almost half show undulose extinction (Fig. 7B). Quartz grains are usually fractured and they are partly deformed due to shearing with clearly visible indicators of displacement (Fig. 7A, H). Secondary biotite has rarely crystallized in the extensive quartz fractures (Fig. 7G, H). Deformed quartz grains contain healed microcracks marked by fluid inclusions (Fig. 6D). Moreover, domino boudins (Fig. 6A) and shearband boudins (Fig. 7E) can be observed for the elongated quartz crystals. Bulging and serrated grain boundaries are present on the quartz grain exteriors, often formed at the contact zone with biotite crystals (Fig. 7C, D).

The biotite flakes range up to 1 mm in length and 150–200  $\mu\text{m}$  in thickness. Most of them show signs of deformation. They are slightly folded, curved or broken and adapt to “bent” quartz grains (Fig. 7B). Certain of the biotite crystals contain intergrowths of needle quartz (Fig. 6H) or zircon inclusions which are fractured and deformed together with whole biotite flakes (Fig. 6E).

Potassic feldspar grains are often ruptured in a similar way to the accompanying quartz grains. The cracks tend to be overgrown with secondary minerals (Fig. 6B).

Additionally disturbed foliation could be observed in the tuffites. Flat-parallel textures consist of biotite flakes, elongated quartz grains and clay matrix (Fig. 6A, C). The foliation is the result of tectonic compression, but has been disturbed by numerous deformation processes, including crenulation cleavage (Fig. 7F).

#### XRD ANALYSIS RESULTS

The XRD investigation of the powdered whole rocks confirmed the occurrence of non-clay minerals in the tuffites, as observed during macroscopic analysis. The occurrence of quartz, potassic feldspar, biotite and barite was recorded.

The analysis of oriented preparations made on clay minerals in the <2  $\mu\text{m}$  size fraction showed that the contents of

smectite in the illite-smectite are very similar (Table 1) and amount to 22% in the lower tuffite and 23% in the upper tuffite. The XRD patterns of the air-dried and glycolated clay fractions indicate a very similar composition of illite-smectite (Fig. 8A, B). In addition, kaolinite was detected in the <2  $\mu\text{m}$  size fraction (Table 1), comprising 1% of the lower tuffite and 18% of the upper tuffite.

#### K-Ar BIOTITE DATING

The biotite dating made using the K-Ar method (Table 2) gave an age of  $292.8 \pm 4.0$  Ma (Early Permian – Cisuralian) for the biotite crystals from the lower tuffite, and an age of  $341.9 \pm 4.3$  Ma – (Mississippian–Visean) for the biotite in the upper tuffite.

### DISCUSSION OF THE RESULTS OBTAINED

#### DISCREPANCY OF THE BIOTITE K-Ar DATES WITH THE AGE OF DEPOSITION

The results of K-Ar dating contrast with the age of the Niewachłów Beds (Fig. 2) in which both tuffite beds occur, which has determined palaeontologically as Upper Silurian (Ludlovian) (Tomczyk, 1962; Kozłowski and Tomczykowa, 1999). It is therefore necessary to consider the processes that may have affected the K-Ar age of the biotite. Previous palaeotemperature studies (Narkiewicz et al., 2010) carried out on Devonian rocks demonstrated that the heating of the basement in the area of occurrence of these rocks did not exceed 100°C. In addition, the dates from the tuffite beds do not have an age counterpart in the diabase from the Bardo Syncline investigated in previous studies (Migaszewski, 2002; Nawrocki et al., 2007, 2013). Data on burial temperatures and subsequent thermal episodes (Bator et al., 2018) indicate that they did not reach a temperature sufficient to cause argon diffusion from biotite, that begins at  $300 \pm 50^\circ\text{C}$  (Mattinson, 1978; Harrison et al., 1985, 2005; Hodges, 1991). Therefore, neither burial temperature nor contact metamorphism related to the Bardo diabase could have had any impact on the rejuvenation of the radiometric age of the biotite.

The discrepancy of the biotite K-Ar dates with the Silurian age of deposition could be due to kaolinitisation of the biotite, which may result in argon release and a decrease in potassium concentration (Stoch and Sikora, 1976; Mitchell and Taka, 1984). Signs of kaolinitization are visible in the Upper Silurian tuffites. We tried to overcome this problem by performing a very careful biotite separation and choosing only fresh crystals for dating, without any signs of kaolinitization. The potassium concentration in the samples of biotite tested is ~6.5% (Table 2), this is a common value for biotite subjected to metamorphic processes and usually does not affect the reliability of K-Ar dating (e.g., Stevens et al., 1982 and references cited therein). Furthermore, according to Jeong et al. (2006), biotite kaolinitization may cause the release of K and Ar from biotite in equal proportions without distorting the dating results. Therefore, although the impact of kaolinitization and other alteration on the K-Ar dating cannot be completely excluded, we conclude that the results obtained are most likely related to the deformation structures found in the biotite and reflect the age of geological events occurring in the history of this rock.

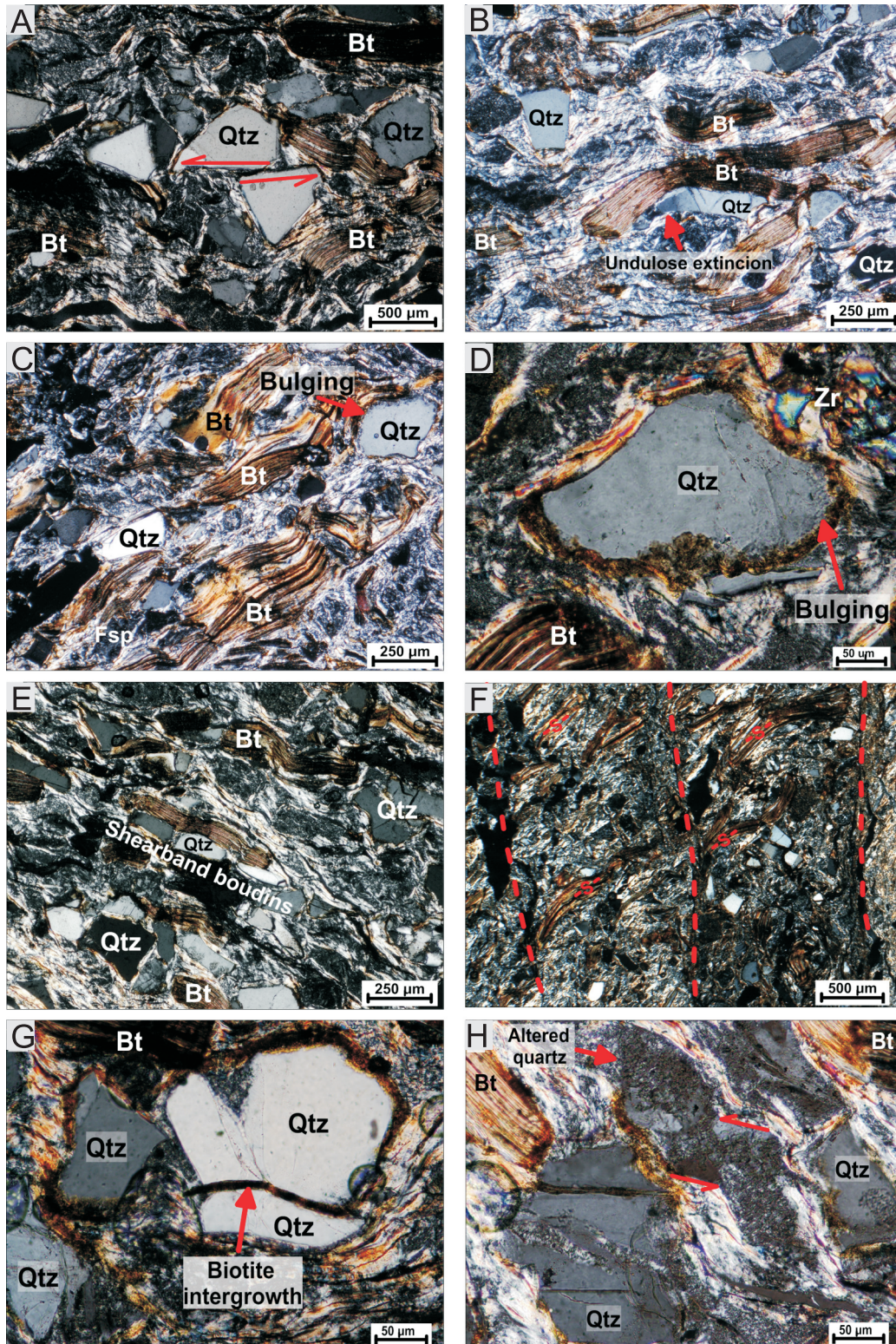


**Fig. 7. Indicators of deformation conditions in the tuffite beds, thin-sections, cross-polarized light**

**A** – shear band type fragmented porphyroblast in quartz grains showing slip – brittle deformation (lower tuffite); **B** – combined ductile deformations of quartz and biotite flakes (lower tuffite); quartz grain in the centre shows undulose extinction; **C** – bulging recrystallization of quartz affected by pressure solution (upper tuffite); **D** – bulging and hydrothermal weakening on the edge of a quartz grain (lower tuffite); **E** – shearband boudins of quartz in a foliation zone – semi-ductile deformation (lower tuffite); **F** – shear bands (crenulation cleavage) and a foliation (S) defined by biotite flakes (upper tuffite); **G** – hydrothermal biotite crystallizing in fractured quartz (lower tuffite); **H** – synkinematic hydrothermal weakening of quartz grain and its ductile deformation (dextral movement indicated by arrows); quartz strongly altered by pressure solution; hydrothermal biotite in fractured quartz (lower tuffite)

TEMPERATURE SETTING  
OF THE DALESZYCE FAULT ZONE

The deformation temperature can be inferred from the co-existence of brittle-ductile deformation structures present in individual mineral grains and their aggregates. This situation applies to potassic feldspars and quartz where, apart from cracks associated with brittle deformation (Figs. 6B and 7A), ductile deformation structures are also visible. These are represented in the tuffites by undulose extinction (Fig. 7B), bulging recrystallisation in quartz (Fig. 7C, D) and shearband boudins (Fig. 7E). These structures indicate deformation in the “bulging recrystallization zone”, which according to generally accepted opinion (Voll, 1976; Dunlap et al., 1997; Dresen et al., 1997; van Daalen et al., 1999; Stipp et al., 2002a, b; Kidder et al., 2013) requires a temperature of at least 250°C. The relatively small amount of bulging recrystallization is a consequence of the lack of triple junctions between the quartz grains (Fig. 7B), promoting, according to Stipp et al. (2002a), the formation of these structures. Moreover, a temperature >250°C is indicated by the presence of crenulation cleavage defined by biotite arrangement (Fig. 7F) in the tuffites (Stesky, 1978). Biotite also occurs in the form of intergrowths in quartz cracks formed during deformation of the tuffites (Fig. 7G, H). This indicates that the biotite in the cracks was formed during heating of the rock in a shear zone and/or migration of hydrothermal fluids. According to Reyes (1990), White and Hedenquist (1995), and Ayati et al. (2008) the minimum temperature of biotite crystallization in hydrothermal conditions is 270–280°C; therefore, in the context of the minimum temperature of quartz deformation (250°C) and the crystallization of hydrothermal biotite in the tuffites, the minimum temperature of heating of this rock can be inferred as ~270°C. The maximum deformation temperature can be inferred from the occurrence of cracks in quartz (Figs. 6A and 7A) and feldspars (Fig. 6B) indicating brittle deformation which, according to Stipp et al. (2002a, b), does not occur above ~300°C. Hence, the rocks underwent deformation at a temperature of ~270–300°C.

Both tuffite layers contain clay minerals, which in low grade metamorphic conditions should be transformed into muscovite at >270°C (Mc Dowell and Elders, 1980). To resolve this problem, X-ray diffraction (XRD) analysis of clay minerals from both layers was performed. The analysis showed the presence of illite-smectite and kaolinite (Fig. 8). The percentage of smectite in the I-S is very similar, respectively: lower tuffite – 22% and upper tuffite – 23% (Table 1). Using the plot of expandability of I-S made by Šucha et al. (1993) for bentonites from the Eastern Slovakia Basin, the maximum palaeotemperature for the tuffites from the HCFB was determined at ~160°C. The results obtained (~160°C) are lower by ~110°C than the minimum deformation temperature of the tuffites inferred from the deformation structures discussed above. In addition, studies by Bator et al. (2018) determined the maximum burial temperature for the Upper Silurian rocks in this area at 100–110°C, which is yet ~50°C lower than the values obtained based on smectite

illitization of the tuffites. Therefore, it seems that the results of palaeotemperature measurements obtained by three different methods are contradictory, and the reaction of smectite to illite can be used to determine temperature in burial diagenetic settings but not to estimate the temperature of fault rock deformation. By reason of these discrepancies, the question should be asked as to which conditions could preserve smectite at >270°C, given that at temperatures >200°C smectite typically changes to illite (Šucha et al., 1993; Abercrombie et al., 1994). One explanation for this phenomenon may be the observations by Junfeng et al. (1997), who found smectite in hydrothermal settings at 285°C. This was supported by the experimental research of Vidal et al. (2012), showing that smectite is stable in hydrothermal conditions at ~300°C. Smectite was also identified by Hirono et al. (2008) and Kuo et al. (2011) in faults in Taiwan, the deformation temperatures of which were determined to be significantly >300°C. Preservation of smectite in these faults in Taiwan was explained by the very short heating time caused by frictional heating or the formation of smectite as a result of a transformation from chlorite in an acidic environment. According to Bustin (1983) and O'Hara (2004), heating caused by fault displacement may take several hours. This is too short a period of time to induce smectite illitization which, according to Whitney (1990), requires several days. Considering the above, it can be supposed that the tuffites analysed from the HCFB were subjected to cataclasis due to reactivation of the Daleszyce Fault Zone. Preservation of smectite in the tuffites can be explained in a similar way as in the fault rocks in Taiwan, i.e. by brief heating (Kuo et al., 2011).

Apart from the frictional heating resulting from displacement along the tuffite layers, hydrothermal solutions may also have been a factor affecting the temperature rise in the deformation zone to values exceeding 270°C. Fluid migration during tectonic activity was responsible for short-term heating of the medium and fluidization of the fault rock. This is indicated by secondary biotite in the cracked quartz (Fig. 7G), fluid inclusions in quartz crystals (Fig. 6D), synkinematic hydrothermal weakening structures in the quartz grains (Fig. 7H), and bulging and serration of grain boundaries (Fig. 7C, D). Furthermore, needle quartz intergrowths in biotite (Fig. 6H) may be associated with hydrothermal conditions (Delvigne, 1998). In addition to the short deformation time, hydrothermal conditions may also have caused increased survival of smectite at high temperatures. We consider that the heating temperature of the tuffites in the 270–300°C range, determined on the basis of deformation of quartz grains, feldspars and biotite, is the correct value, and in the conditions described above could not lead to the transformation of clay minerals. The deformation temperature in the range of ~270–300°C proved sufficient to begin Ar diffusion from biotite, which started at a temperature of 300 ± 50°C (Mattinson, 1978; Harrison et al., 1985, 2005; Hodges, 1991). Moreover, the hydrothermal fluids mentioned above led to retrograde reactions, recrystallization and dissolution during deformation of the tuffites. Such fluid – rock reactions could cause <sup>40</sup>Ar loss and isotopic resetting of the K-Ar age even below the normally used blocking temperature for biotite (de Jong et al., 2009; Villa, 2010; Bosse and Villa, 2019). Therefore, the temperature conditions were sufficient for the rejuvenation of the radiometric age of the Upper Silurian tuffites. The process of rejuvenation of the biotite age proceeded differently in the lower and upper tuffite layers. It can be inferred that the temperature increase in both layers did not occur simultaneously. In the Early Permian, the temperature of the upper tuffite was lower than the deformation temperature of the lower tuffite and did not reach the minimum temperature necessary for the rejuvenation of the biotite K-Ar system. Thin-section analysis shows that the upper

Table 1

XRD results of clay minerals composition, fraction <2 μm

| Sample        | Illite–smectite R1 |      | Kaolinite |  | Sum |
|---------------|--------------------|------|-----------|--|-----|
|               | % smectite         | wt.% | wt.%      |  |     |
| Upper tuffite | 23                 | 82   | 18        |  | 100 |
| Lower tuffite | 22                 | 99   | 1         |  | 100 |

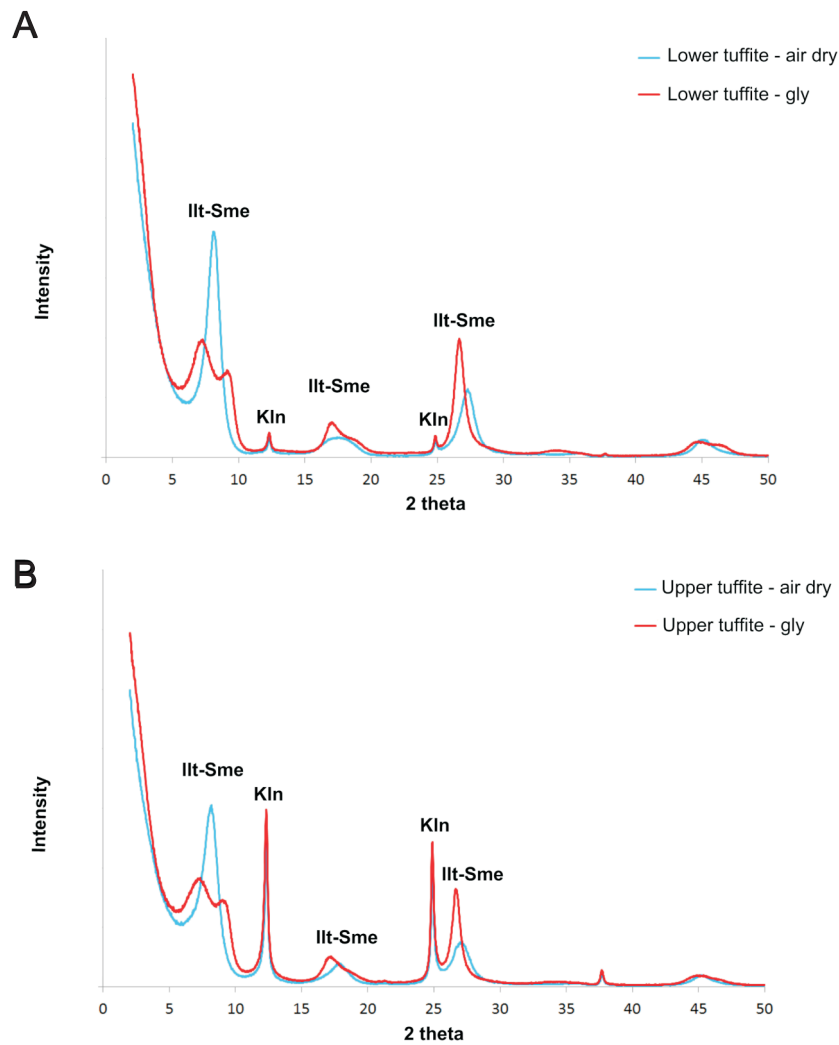


Fig. 8. XRD patterns of the <2 mm size fractions of samples under natural air-dried and ethylene glycol saturated conditions

A – lower tuffite, B – upper tuffite; Ill – illite, Sme – smectite, Kln – kaolinite

tuffite (Fig. 7F) has been subjected to much stronger cataclasis than the lower tuffite (Fig. 6A). This is evident in the upper tuffite composition which contains 3 times more clay matrix, consisting mainly of illite-smectite and kaolinite (Fig. 8), than the lower tuffite. The presence of smectite reduced friction in the fault zone, which meant that the deformation temperature (caused by frictional heating) could not exceed 180°C (Haines and van der Pluijm, 2012; Oohashi et al., 2015; Schleicher et al., 2015). Therefore the lower deformation temperature of the upper tuffite layer in the Early Permian was most likely related to the higher content of clay matrix in the rock. Clay minerals reduced the friction between quartz and feldspar grains, preventing

them from overheating and giving this layer the characteristics of a “weak fault zone” (Wintsch et al., 1995; Rutter et al., 2001; Rice, 2006; Carpenter et al., 2011; Holdsworth et al., 2011). The same clay minerals most likely reduced the permeability of the upper tuffite layer. According to Caine et al. (1996), Gray et al. (2005), Walker et al. (2013), Boulton et al. (2017), Nenoen et al. (2019) the presence of clay minerals within a fault core could decrease hydrothermal fluid flow. Therefore it seems that reduced hydrothermal fluid flow can eliminate the effect of hydrothermal heating and decrease the tendency of the biotite to Ar diffusion. Thus, the lack of, or lesser, hydrothermal heating in the upper tuffite layer during the second stage of deformation

Table 2

#### Results of the tuffite dating with K-Ar methods

| Sample        | $^{40}\text{Ar}/^{38}\text{Ar}$ | $^{36}\text{Ar}/^{40}\text{Ar}$ [x1000] | $^{38}\text{Ar}_{\text{spike}}$ [pmol] | m [mg] | $\%^{40}\text{Ar}_{\text{rad}}$ | $^{40}\text{Ar}_{\text{rad}}$ [nmol/g] | %K   | Age [Ma]   |
|---------------|---------------------------------|-----------------------------------------|----------------------------------------|--------|---------------------------------|----------------------------------------|------|------------|
| Upper tuffite | 2.4028                          | 0.171                                   | 65.99                                  | 35.6   | 94.9                            | 4.229                                  | 6.48 | 341.9 ±4.3 |
| Lower tuffite | 2.0797                          | 0.205                                   |                                        | 35.49  | 93.9                            | 3.633                                  | 6.59 | 292.8 ±4.0 |

Table 3

**Comparison of radiometric age data for magmatic rocks from the Holy Cross Fold Belt, Kraków-Lubliniec Fault Zone, East European Platform and the Sudetes**

| Site                       |                             | Lithology           | Material        | Method     | Age [Ma]       | Epoch                    | Reference                                  |                                                  |
|----------------------------|-----------------------------|---------------------|-----------------|------------|----------------|--------------------------|--------------------------------------------|--------------------------------------------------|
| Trans European Suture Zone | Holy Cross Fold Belt        | Wszachów-4*         | lamprophyre     | biotite    | K-Ar           | 275.0 ±15                | Cisuralian (P1)                            | <a href="#">Migaszewski (2002)</a>               |
|                            |                             | Wszachów-4*         | lamprophyre     | biotite    | K-Ar           | 288.8 ±15                | Cisuralian (P1)                            | <a href="#">Migaszewski (2002)</a>               |
|                            |                             | Janowice-2*         | diabase         | zircon     | U-Pb           | 300.0 ±10                | Late Pennsylvanian (C2/P1)                 | <a href="#">Krzemińska and Krzemiński (2019)</a> |
|                            |                             | Góra Salkowa        | lamprophyre     | biotite    | K-Ar           | 347.8 ±15                | Early Mississippian (C1)                   | <a href="#">Migaszewski (2002)</a>               |
|                            |                             | Kolonia-2*          | lamprophyre     | biotite    | K-Ar           | 351.2 ±15                | Early Mississippian (C1)                   | <a href="#">Migaszewski (2002)</a>               |
|                            |                             | Milejowice-1*       | diabase         | whole rock | Ar/Ar          | 331.0 ±1.9               | Middle Mississippian (C1)                  | <a href="#">Nawrocki et al. (2013)</a>           |
|                            | Dolsk Fault Zone            | Zdrój-1*            | dacite lava     | zircon     | U-Pb           | 296 ±3                   | Cisuralian (P1)                            | <a href="#">Breitkreuz et al. (2007)</a>         |
|                            | Kraków-Lubliniec Fault Zone | Zalas               | rhyodacite      | zircon     | U-Pb           | 295.1 ±2.6               | Cisuralian (P1)                            | <a href="#">Nawrocki et al. (2008)</a>           |
|                            |                             | 16-WB-424*          | rhyodacite      | whole rock | Ar/Ar          | 294.4 ±1.6               | Cisuralian (P1)                            | <a href="#">Nawrocki et al. (2010)</a>           |
|                            |                             | Dubie Quarry        | andesite        | amphibole  | K-Ar           | 291.3 ±6.4               | Cisuralian (P1)                            | <a href="#">Lewandowska et al. (2007)</a>        |
|                            |                             | WB-137-436*         | diabase         | whole rock | Ar/Ar          | 331.3 ±3.6               | Middle Mississippian (C1)                  | <a href="#">Nawrocki et al. (2010)</a>           |
|                            | East European Platform      | Daszewo 12*         | rhyolite        | zircon     | U-Pb           | 293.0 ±2.3               | Cisuralian (P1)                            | <a href="#">Breitkreuz et al. (2007)</a>         |
|                            |                             | Parczew IG 9*       | alkaline basalt | whole rock | Ar/Ar          | 338.5 ±0.7               | Early Mississippian (C1)                   | <a href="#">Pańczyk and Nawrocki (2015)</a>      |
|                            |                             | Pisz*               | gabbro          | zircon     | U-Pb           | 345.5 ±5                 | Early Mississippian (C1)                   | <a href="#">Krzemińska et al. (2006)</a>         |
|                            |                             | Elk IG4*            | syenite         | zircon     | U-Pb           | 347.7 ±7                 | Early Mississippian (C1)                   | <a href="#">Krzemińska et al. (2006)</a>         |
| Sudetes                    | Wielistawka                 | rhyolite            | zircon          | U-Pb       | 292.8 ±2.1     | Cisuralian (P1)          | <a href="#">Awdankiewicz et al. (2014)</a> |                                                  |
|                            | Łażany                      | granodiorite        | zircon          | U-Pb       | 294.4 ±2.7     | Cisuralian (P1)          | <a href="#">Tumiak et al. (2014)</a>       |                                                  |
|                            | Žulová Pluton               | quartz monzodiorite | zircon          | U-Pb       | 292 ±4         | Cisuralian (P1)          | <a href="#">Laurent et al. (2014)</a>      |                                                  |
|                            | Laski/Mąkolno               | diorite             | zircon          | U-Pb       | 349.0 ±3.4/3.7 | Early Mississippian (C1) | <a href="#">Jokubauskas et al. (2018)</a>  |                                                  |
|                            | Przedborowa                 | monzodiorite        | zircon          | U-Pb       | 341.8 ±1.9     | Early Mississippian (C1) | <a href="#">Pietranik et al. (2013)</a>    |                                                  |
|                            | Jordanów Quarry             | granite             | zircon          | U-Pb       | 337 ±4         | Early Mississippian (C1) | <a href="#">Kryza (2011)</a>               |                                                  |
|                            | 2/II Leszno Dolne*          | granodiorite        | Zircon          | U-Pb       | 344.4 ±1       | Early Mississippian (C1) | <a href="#">Dörr et al. (2006)</a>         |                                                  |

\* - borehole

The age of magmatism corresponding to the age of the lower tuffite metamorphism (292.8 ±4.0 Ma) – this study

The age of magmatism corresponding to the age of the upper tuffite metamorphism (341.9 ±4.3 Ma) – this study

was superimposed on lesser frictional heating and together these factors contributed to the preservation of the older Mississippian radiometric age of the biotite. [Yamada and Mizoguchi \(2011\)](#) and [Yang et al. \(2016\)](#) have showed that even 15 cm from the edge of a fault, the rock temperature may be several hundred degrees lower than at its core. It follows that the distance between the two tuffites, amounting to 80 cm in the section ([Fig. 4B](#)), was sufficient so that heating one layer did not affect the temperature of the other.

To summarize, Early Carboniferous activation of the DFZ associated with displacements along both tuffite layers led to rejuvenation of the biotite age. Geomechanical differences between the tuffites (the lower one with more coarse-grained ma-

terial; the upper one with more clay matrix) meant that, during the Early Permian reactivation of the DFZ, only the lower tuffite was heated and rejuvenated again.

A feature of the K-Ar dating method is that it does not allow complete exclusion of a partial reset of the radiometric age of the minerals and rocks studied (see: [Arehart et al., 1993](#); [Kellet et al., 2016](#); [Barnes et al., 2020](#)). However, our analysis of the fault metamorphism conditions clearly indicates that these could be sufficient for complete rejuvenation of the radiometric age of the K-Ar biotite from the Niewachłów tuffites. In order to make sure that the results obtained have geological significance, below we compare them with the occurrence of magmatism in the HCFB and in adjacent areas.

## TECTONIC ACTIVITY OF THE DFZ IN THE CONTEXT OF REGIONAL MAGMATISM

The occurrence of two different dates for tuffite beds situated only 80 cm away from each other in vertical succession points to their connection with two different deformational stages in the DFZ. The first stage took place in the Mississippian and the second one occurred during the Early Permian.

The ages for the DFZ displacements obtained have age counterparts in the magmatic activity and metamorphism reported from the HCFB and adjacent areas (Table 3). It is possible to distinguish numerous magmatic intrusions formed at similar times, such as the Lower Carboniferous lamprophyre from the Kolonia 2 borehole in Góra Salkowa near Daleszyce within the HCFB (Migaszewski, 2002), as well as the diabase from the WB 137-436 borehole (Table 3) in the Kraków-Lubliniec Fault Zone (Nawrocki et al., 2010), being the boundary between the Małopolska Block and Brunovistulicum. The same Mississippian age was determined for an alkaline basalt (Table 3) from the Parczew IG 9 borehole (Pańczyk and Nawrocki, 2015) in the Lublin Basin located within the TESZ area, as well as for a gabbro from the Pisz intrusion and a syenite from the Elk intrusion (Krzemińska et al., 2006) situated in NE Poland on the Eastern European Platform. An Early Carboniferous age of magmatism has also been recorded in the Sudetes region (Table 3) for diorites from the Kłodzko-Złoty Stok intrusion (Jokubauskas et al., 2018), monzodiorites from the Niemcza Zone (Pietranik et al., 2013), granitoid dykes from the Ślęza ophiolite (Kryza, 2011) and granodiorites and monzodiorites of the Odra Fault Zone (Dörr et al., 2006).

Displacements along the DFZ dated to the Early Permian (Cisuralian) are correlated in the HCFB area (Migaszewski, 2002) with (Table 3) a lamprophyre from the Wszachów 4 and a diabase from the Janowice 2 borehole (Krzemiński and Krzemińska, 2019). In adjacent areas (Table 3), similar results were obtained from a rhyodacite (Nawrocki et al., 2008, 2010) and an andesite related to the Kraków-Lubliniec Fault Zone (Lewandowska et al., 2007) and a dacite occurring slightly farther to the west (Breitkreuz et al., 2007), related to the Dolsk Fault Zone. A similar age (Table 3) was also recorded (Breitkreuz et al., 2007) for a rhyolite from the Daszewo 12 borehole situated on the East European Platform in northern Poland. In addition, numerous magmatic intrusions in the Sudetes have been determined as Early Permian (Table 3). There are, among others: rhyolites of the North Sudetes Basin (Awdankiewicz et al., 2014); a granodiorite on the Strzegom-Sobótka Massif (Turniak et al., 2014); and granitoids, granodiorites and monzodiorites of the Žulová Pluton (Laurent et al., 2014).

Both the Mississippian and Early Permian dates quoted are typical of the final phases of the Variscan orogeny in Central Europe (Aleksandrowski et al., 1997; Mazur et al., 2006). The first stage of deformation of the basement took place exceptionally early, i.e., still during the deposition of clastic rocks within the HCFB that lasted until the Late Visean (Szulczewski, 1995; Racki, 2006). Studies of the palaeomagmatism of the HCFB area have showed that tectonic events, which resulted in numerous episodes of remagnetisation of the sedimentary rocks of the Kielce region, occurred in the Mississippian and Early Permian (Lewandowski, 1999; Grabowski and Nawrocki, 2001; Zwing, 2003; Grabowski et al., 2006, 2009; Szaniawski et al., 2011). According to Szaniawski (2008), these two intervals should be assigned to two stages of the Variscan deformation

in the Holy Cross Mountains. Considering this geological context, dating of movements along the DFZ reflects the ages of the two phases related to the Variscan orogeny within the HCFB, when this fault became reactivated. These two tectonic events occurred during the Mississippian ( $341.9 \pm 4.3$  Ma) and the Early Permian ( $292.8 \pm 4.0$  Ma).

The Mississippian age of the DFZ deformation correlates well with the age of the intrusion of alkaline basalt noted above (Table 3) encountered in boreholes within the Lublin Basin (Pańczyk and Nawrocki, 2015) near the TESZ. The area where alkaline basalts occur is separated from the HCFB by the Radom-Kraśnik Block, which also belongs to the TESZ. In the Radom-Kraśnik Block, Krzywiec et al. (2017a, b, 2018) identified the presence of Variscan deformation structures. It is plausible that the Mississippian deformation of the DFZ reflects relative tectonic displacements of the Małopolska Block, the Łysogóry Block and the Radom-Kraśnik Block. The reactivation of the DFZ during the Early Permian also corresponds in time with the formation of magmatic rocks within the TESZ and adjacent areas (Table 3). These two stages of magmatic and tectonic activity are also indicated by the dating of the K-Ar illitization of smectite made by Kowalska et al. (2019) in the Polish part of the East European Platform. This research indicates that the maximum heating in the area took place in the Mississippian and Early Permian, which correspond to the Sudetian and the Asturian phases of the Variscan Orogen respectively. According to Żelaźniewicz et al. (2016), overthrusting of the foreland of the Variscides onto the TESZ led to the activation of the bounding fault and triggered magmatism. In this case, an echo of the distant displacements at the TESZ boundary faults was the activation of minor faults, such as the Daleszyce Fault Zone.

## CONCLUSIONS

Radiometric dating of biotite from the newly discovered Niewachłów tuffites occurring within Silurian greywackes (Niewachłów Beds of Ludlow age) revealed Early Permian and Mississippian ages. The discrepancy between the biotite K-Ar ages and the Late Silurian depositional age of the tuffites may indicate the rejuvenation of the radiometric age of the biotite, which occurred in 2 phases:

- $341.9 \pm 4.3$  [Ma] (upper tuffite) corresponding to the Mississippian (Visean);
- $292.8 \pm 4.0$  [Ma] (lower tuffite), corresponding to the Early Permian (Cisuralian).

The rejuvenation of the radiometric age of the biotite may have resulted from the reactivation of the DFZ which “utilized” Niewachłów tuffites as a “weak zone”. Simultaneously with this reactivation, migration of hydrothermal fluids responsible for frictional/hydrothermal heating to temperatures of 270-300°C took place. The presence of hydrothermal fluids may have facilitated lowering of the biotite closure temperature.

The two distinct tuffite beds, situated only 80 cm apart, may record different events due to geomechanical differences resulting from different rock texture and clay content.

The reactivation of, and deformation along, the Daleszyce Fault Zone may be considered as a result of lithospheric block movements inside the TESZ during the Late Variscan reconstruction of the Baltica palaeocontinent margin.

**Acknowledgements.** The research was supported with funds from the Statutory Activity of the DSM 2017 No 115620 Faculty of Geology, University of Warsaw. The authors would like to thank S. Hałas and A. Wójtowicz from the Institute of Physics, Maria Curie-Skłodowska University, for K-Ar analysis. We are grateful to E. Jurewicz for her numerous insightful comments and explanations in the fields of petrotectonics and structural geology, M. Szczërba and G. Kaproń for much advice in the interpretation of clay mineral composition. We would like to express

our gratitude to K. Walczak, T. Bajda, I. Broska and five anonymous reviewers for critical and constructive reviews of the manuscript. The authors would like to thank the anonymous reviewer for extensive comments and discussions on the interpretation of K-Ar dating in the light of tectonic and hydrothermal activity, biotite characteristics and the Ar diffusion processes. We are grateful to the owners of the excavation with tuffites in Czyżów village, for their great patience and fieldwork permission.

## REFERENCES

- Abercrombie, H.J., Hutcheon, I.E., Bloch, J.D., de Caritat, P., 1994.** Silica activity and the smectite-illite reaction. *Geology*, **22**: 539–542.
- Aleksandrowski, P., Mazur, S., 2017.** On the new tectonic solutions in Geological Atlas of Poland (in Polish with English summary). *Przegląd Geologiczny*, **65**: 1499–1510.
- Aleksandrowski, P., Kryza, R., Mazur, S., Żaba, J., 1997.** Kinematic data on major Variscan strike-slip faults and shear zones in the Polish Sudetes, northeast Bohemian Massif. *Geological Magazine*, **133**: 727–739.
- Arehart, G.B., Foland, K.A., Naeser, C.W., Kesler, S.E., 1993.**  $^{40}\text{Ar}/^{39}\text{Ar}$ , K/Ar and fission track geochronology of sediment-hosted disseminated gold deposits at Post-Betze, Carlin trend, northeastern Nevada. *Economic Geology*, **88**: 622–646.
- Awdankiewicz, M., Kryza, R., Szczepara, N., 2014.** Timing of post-collisional volcanism in the eastern part of the Variscan Belt: constraints from SHRIMP zircon dating of Permian rhyolites in the North-Sudetic Basin (SW Poland). *Geological Magazine*, **151**: 611–628.
- Ayati, F., Yavuz, F., Noghreyan Haroni, H.A., Yavuz, R., 2008.** Chemical characteristics and composition of hydrothermal biotite from the Dalli porphyry copper prospect, Arak, central province of Iran. *Mineralogy and Petrology*, **94**: 107–122.
- Barnes, C.J., Jeanneret, P., Kullerud, K., Majka, J., Schneider, D., A., Bukala, M., Klonowska, I., 2020.** Exhumation of the high-pressure Tsäkkok Lens, Swedish Caledonides: insights from the structural and white mica  $^{40}\text{Ar}/^{39}\text{Ar}$  geochronological record. *Tectonics*, **39**: 1–23.
- Bator, D., Anczkiewicz, A., Dunkl, I., Golonka, J., Paszkowski, M., Mazur, S., 2018.** Tectonothermal history of the Holy Cross Mountains (Poland) in light of low-temperature thermochronology. *Terra Nova*, **30**: 270–278.
- Bednarczyk, W., Chlebowski, R., Kowalczewski, Z., 1966.** Ordovician in the Bardo Syncline (Święty Krzyż Mts.) (in Polish with English summary). *Geological Quarterly*, **10** (3): 705–723.
- Belka, Z., Valverde-Vaquero, P., Dörr, W., Ahrendt, H., Wemmer, K., Franke, W., 2002.** Accretion of first Gondwana-derived terranes at the margin of Baltica. *Geological Society Special Publications*, **201**: 19–36.
- Berthelsen, A., 1992.** From Precambrian to Variscan Europe. In: *A Continent Revealed – the European Geotraverse* (eds. D.J. Blundell, R. Freeman and S. Mueller): 153–164. Cambridge University Press, Cambridge.
- Breitkreuz, C., Kennedy, A., Geißler, M., Ehling, B.C., Kopp, J., Muszyński, A., Protas, A., Stouge, S., 2007.** Far Eastern Avalonia: its chronostratigraphic structure revealed by SHRIMP zircon ages from Upper Carboniferous to Lower Permian volcanic rocks (drill cores from Germany, Poland and Denmark). *GSA Special Paper*, **423**: 173–190.
- Bosse, V., Villa, I.M., 2019.** Petrochronology and hydrochronology of tectono-metamorphic events. *Gondwana Research*, **71**: 76–90.
- Boulton, C., Menzies, C.D., Toy, V.G., Townend, J., Sutherland, R., 2017.** Geochemical and microstructural evidence for interseismic changes in fault zone permeability and strength, Alpine Fault, New Zealand. *Geochemistry, Geophysics, Geosystems*, **18**: 238–265.
- Bustin, R.M., 1983.** Heating during thrust faulting in the Rocky Mountains: friction or fiction. *Tectonophysics*, **95**: 309–328.
- Caine, J.S., Evans, J.P., Forster, C.B., 1996.** Fault zone architecture and permeability structure. *Geology*, **24**: 1025–1028.
- Carpenter, B.M., Marone, C., Saffer, D.M., 2011.** Weakness of the San Andreas Fault revealed by samples from the active fault zone. *Nature Geoscience*, **4**: 251–254.
- Czarnocki, J., 1919.** Stratygrafia i tektonika Gór Świętokrzyskich (in Polish). *Prace Towarzystwa Naukowego Warszawskiego*, **28**: 1–172.
- Czarnocki, J., 1928.** Profil dolnego i górnego ordowiku w Zalesiu pod Łagowem w porównaniu z ordowikiem innych miejscowości środkowej części Gór Świętokrzyskich (in Polish). *Sprawozdania Państwowego Instytutu Geologicznego*, **4**: 555–568.
- Czarnocki, J., 1936.** Überblick der Stratigraphie und Paläogeographie des Unterdevons im Polnischen Mittelgebirge (in Polish with German summary). *Sprawozdania Państwowego Instytutu Geologicznego*, **8**: 1–27.
- Czarnocki, J., 1939.** Field work in the święty Krzyż Mountains in 1938 (in Polish with English summary). *Biuletyn Państwowego Instytutu Geologicznego*, **15**: 1–27.
- Czarnocki, J., 1957.** Tectonics of the Święty Krzyż Mountains. *Geology of the Lysogóry Region* (in Polish with English summary). *Prace Instytutu Geologicznego*, **18**: 11–138.
- Czarnocki, J., 1958.** Mapa rozmieszczenia diabazów w okolicy Łagowa (in Polish). *Prace Instytutu Geologicznego*, **21**.
- Cox, A., Dalrymple, G.B., 1967.** Statistical analysis of geomagnetic reversal data and the precision of potassium-argon dating. *Journal of Geophysical Research*, **72**: 2603–2614.
- Dadlez, R., 2001.** Holy Cross Mts. area – crustal structure, geophysical data and general geology. *Geological Quarterly*, **45** (2): 99–106.
- Dadlez, R., Kowalczewski, Z., Znosko, J., 1994.** Some key problems of the pre-Permian tectonics of Poland. *Geological Quarterly*, **38** (2): 169–190.
- de Jong, K., Wang, B., Faure, M., Shu, L., Cluzel, D., Charvet, J., Ruffet, G., Chen, Y., 2009.** New  $^{40}\text{Ar}/^{39}\text{Ar}$  age constraints on the Late Palaeozoic tectonic evolution of the western Tianshan (Xinjiang, northwestern China), with emphasis on Permian fluid ingress. *International Journal of Earth Sciences*, **98**: 1239–1258.
- Delvigne, J.E., 1998.** Atlas of micromorphology of mineral alteration and weathering. *Canadian Mineralogist Special Publication*, **3**.
- Dörr, W., Żelaźniewicz, A., Bylina, P., Schastok, J., Franke, W., Haack, U., Kulicki, C., 2006.** Tournaisian age of granitoids from the Odra Fault Zone (southwestern Poland): equivalent of the Mid-German Crystalline High? *International Journal of Earth Sciences*, **95**: 341–349.

- Dresen, G., Duyster, J., Stöckhert, B., Wirth, R., Zulauf, G., 1997.** Quartz dislocation microstructure between 7000 m and 9100 m depth from the Continental Deep Drilling Program. *KTB*, **102**: 18443–18452.
- Dunlap, W.J., Hirth, G., Teyssier, C., 1997.** Thermomechanical evolution of a ductile duplex. *Tectonics*, **16**: 983–1000.
- Filonowicz, P., 1976.** Objasnienia do szczegółowej mapy geologicznej Polski 1:50 000, arkusz Daleszyce (in Polish). Wyd. Geol., Warszawa.
- Gagała, Ł., 2005.** Pre-Ordovician polyphase tectonics of the Cambrian sequences in the Kielce Unit, Holy Cross Mts. (Central Poland). *Geological Quarterly*, **49** (1): 53–66.
- Gagała, Ł., 2015.** Late Silurian deformation in the Łysogóry Region of the Holy Cross Mountains revisited: restoration of a progressive Caledonian unconformity in the Klonów Anticline and its implications for the kinematics of the Holy Cross Fault (central Poland). *Geological Quarterly*, **59** (3): 441–456.
- Grabowski, J., Nawrocki, J., 2001.** Palaeomagnetism of some Devonian carbonates from the Holy Cross Mts. (Central Poland): large pre-Permian rotations or strain modified palaeomagnetic directions? *Geological Quarterly*, **45** (2): 165–178.
- Grabowski, J., Narkiewicz, M., Sobieñ, K., 2006.** Thermal controls on the remagnetization of Devonian carbonate rocks in the Kielce region (Holy Cross Mts) (in Polish with English summary). *Przegląd Geologiczny*, **54**: 895–904.
- Grabowski, J., Narkiewicz, M., Szaniawski, R., Resak, M., Littke, R., 2009.** Late Variscan tectonothermal history of the Holy Cross Mts. (Central Poland) as revealed by integrated palaeomagnetic and 1-D basin modelling study. EGU General Assembly; Geophysical Research Abstracts, **11**.
- Grad, M., Janik, T., Yliniemi, J., Guterch, A., Luosto, U., Tiira, T., Komminaho, K., Oeroda, P., Höing, K., Makris, J., Lund, C.E., 1999.** Crustal structure of the Mid-Polish Trough beneath the Teisseyre-Tornquist Zone seismic profile. *Tectonophysics*, **314**: 145–160.
- Grad, M., Guterch, A., Mazur, S., 2002.** Seismic refraction evidence for crustal structure in the central part of the Trans-European Suture Zone in Poland. *Geological Society Special Publications*, **201**: 295–309.
- Gray, M.B., Stamatakos, J.A., Ferrill, D.A., Evans, M.A., 2005.** Fault-zone deformation in welded tuffs at Yucca Mountain, Nevada, USA. *Journal of Structural Geology*, **27**: 1873–1891.
- Haines, S., van der Pluijm, B., 2012.** Patterns of mineral transformations in clay gouge, with examples from low-angle normal fault rocks in the western USA. *Journal of Structural Geology*, **43**: 2–32.
- Hałas, S., 1995.** Geochronologia izotopowa oparta na rozpadzie promieniotwórczym potasu-40 (in Polish). *Przegląd Geologiczny*, **43**: 993–998.
- Harrison, T.M., Duncan, I., Mc Dougall, I., 1985.** Diffusion of <sup>40</sup>Ar in biotite: temperature, pressure and compositional effects. *Geochimica et Cosmochimica Acta*, **49**: 2461–2468.
- Harrison, T.M., Grove, M., Lovera, O.M., Zeitler, P.K., 2005.** Continuous thermal histories from inversion of closure profiles. Reviews in Mineralogy and Geochemistry, **58**: 389–409.
- Hirono, T., Fujimoto, K., Yokoyama, T., Hamada, Y., Tanikawa, W., Tadai, O., Mishima, T., Tanimizu, M., Lin, W., Soh, W., Song, S.R., 2008.** Clay mineral reactions caused by frictional heating during an earthquake: an example from the Taiwan Chelungpu fault. *Geophysical Research Letters*, **35**: L16303.
- Hodges, K.V., 1991.** Pressure-temperature-time paths. *Annual Review of Earth and Planetary Sciences*, **19**: 207–236.
- Holdsworth, R.E., van Diggelen, E.W.E., Spiers, C.J., de Bresser, J.H.P., Walker, R.J., Bowen, L., 2011.** Fault rocks from the SAFOD core samples: implications for weakening at shallow depths along the San Andreas Fault, California. *Journal of Structural Geology*, **33**: 132–144.
- Jeong, G.Y., Cheong, C.S., Kim, J., 2006.** Rb-Sr and K-Ar systems of biotite in surface environments regulated by weathering processes with implications for isotopic dating and hydrological cycles of Sr isotopes. *Geochimica et Cosmochimica Acta*, **70**: 4734–4749.
- Jokubauskas, P., Bagiński, B., Macdonald, R., Krzemińska, E., 2018.** Multiphase magmatic activity in the Variscan Kłodzko-Złoty Stok intrusion, Polish Sudetes: evidence from SHRIMP U-Pb zircon ages. *International Journal of Earth Sciences*, **107**: 1623–1639.
- Junfeng, J., Browne, P.R.L., Yingjun, L., 1997.** Occurrence of mixed-layer illite/smectite at temperature of 285°C in an active hydrothermal system and its significance. *Chinese Science Bulletin*, **42**: 318–321.
- Kardymowicz, I., 1957.** On the petrography of the diabase of the Święty Krzyż Mountains (in Polish with English summary). *Geological Quarterly*, **1** (1): 139–154.
- Kardymowicz, I., 1962.** Petrological studies of the lamprophyres in the Święty Krzyż Mountains (in Polish with English summary). *Geological Quarterly*, **6** (3): 271–311.
- Kellett, D.A., Warren, C., Larson, K.P., Zwingmann, H., van Staal, C., Rogers, N., 2016.** Influence of deformation and fluids on Ar retention in white mica, dating the Dover Fault, Newfoundland Appalachians. *Lithos*, **254–255**: 1–17.
- Kidder, S., Avouac, J.P., Chan, Y.C., 2013.** Application of titanium-in-quartz thermobarometry to greenschist facies veins and recrystallized quartzites in the Hsüehshan range, Taiwan. *Solid Earth*, **4**: 1–21.
- Konon, A., 2007.** Strike-slip faulting in the Kielce Unit, Holy Cross Mountains, central Poland. *Acta Geologica Polonica*, **57**: 415–441.
- Konon, A., 2008.** Tectonic subdivision of Poland: Holy Cross Mountains and adjacent areas (in Polish with English summary). *Przegląd Geologiczny*, **56**: 921–926.
- Kowalczewski, Z., Lisik, R., 1974.** New data on diabases and geological structure of the Prągowiec area in the Góry Świętokrzyskie Mts. (in Polish with English summary). *Biuletyn Instytutu Geologicznego*, **275**: 113–158.
- Kowalczewski, Z., Rubinowski, Z., 1962.** Główne elementy tektoniczne paleozoiku antyklinorium świętokrzyskiego (in Polish). *Przegląd Geologiczny*, **10**: 451–455.
- Kowalczewski, Z., Rup, M., 1989.** Zechstein rocks of the Góry Świętokrzyskie (in Polish with English summary). *Biuletyn Państwowego Instytutu Geologicznego*, **362**: 5–39.
- Kowalczewski, Z., Żylińska, A., Szczepaniak, Z., 2006.** Kambr w Górach Świętokrzyskich (in Polish). In: *Procesy i zdarzenia w historii geologicznej Gór Świętokrzyskich* (eds. S. Skompski and A. Żylińska): 14–27. LXXVII Zjazd Naukowy Polskiego Towarzystwa Geologicznego, Ameliówka k. Kielc, 28–30 czerwca 2006 r. Polskie Towarzystwo Geologiczne, Państwowy Instytut Geologiczny, Wydział Geologii Uniwersytetu Warszawskiego.
- Kowalska, S., Wójtowicz, A., Hałas, S., Wemmer, K., Mikołajewski, Z., Buniak, A., 2019.** Thermal history of Lower Palaeozoic rocks from the East European Platform margin of Poland based on K-Ar age dating and illite-smectite palaeothermometry. *Annales Societatis Geologorum Poloniae*, **89**: 481–509.
- Kozłowski, W., Tomczykowa, E., 1999.** A new occurrence of benthic fauna in the Niewachłów Greywackes (Upper Silurian) from Zalesie near Łagów in the Holy Cross Mountains. *Geological Quarterly*, **43** (1): 129–126.
- Kozłowski, W., Domańska-Siuda, J., Nawrocki, J., 2014.** Geochemistry and petrology of the upper Silurian greywackes from the Holy Cross Mountains (Central Poland): implications for the Caledonian history of the southern part of the Trans-European Suture Zone (TESZ). *Geological Quarterly*, **58** (2): 311–336.
- Kryza, R., 2011.** Early Carboniferous (~337 Ma) granite intrusion in Devonian (~400 Ma) ophiolite of the Central-European Variscides. *Geological Quarterly*, **55** (3): 213–222.
- Krzemińska, E., Krzemiński, L., 2019.** Magmatic episodes in the Holy Cross Mountains, Poland – a new contribution from multi-age zircon populations. *Biuletyn Państwowego Instytutu Geologicznego*, **474**: 43–58.
- Krzemińska, E., Wiszniewska, J., Williams, I.S., 2006.** Early Carboniferous age of the cratonic intrusions in the crystalline basement of NE Poland. *Przegląd Geologiczny*, **54**: 1093–1098.

- Krzemiński, L., 2004.** Geochemical constraints on the origin of the mid-Palaeozoic diabases from the Holy Cross Mts. and Upper Silesia, south eastern Poland. *Geological Quarterly*, **48** (2): 147–158.
- Krzywiec, P., Gaęła, Ł., Mazur, S., Słonka, Ł., Kufraś, M., Malinowski, M., Pietsch, K., Golonka, J., 2017a.** Variscan deformation along the Teisseyre-Tornquist Zone in SE Poland: thick-skinned structural inheritance or thin-skinned thrusting? *Tectonophysics*, **718**: 83–91.
- Krzywiec, P., Mazur, S., Gaęła, Ł., Kufraś, M., Lewandowski, M., Malinowski, M., Buffenmyer, V., 2017b.** Late Carboniferous thin-skinned compressional deformation above the SW edge of the East European Craton as revealed by reflection seismic and potential fields data – correlations with the Variscides and the Appalachians. *GSA Memoir*, **213**: 353–372.
- Krzywiec, P., Kufraś, M., Gaęła, Ł., Mazur, S., Słonka, Ł., 2018.** Variscan (late Carboniferous) tectonics of the SE Lublin Basin. *Geology, Geophysics and Environment*, **44**: 145–202.
- Kuo, L.W., Song, S.R., Huang, L., Yeh, E.C., Chen, H.F., 2011.** Temperature estimates of coseismic heating in clay-rich fault gouges, the Chelungpu fault zones, Taiwan. *Tectonophysics*, **502**: 315–327.
- Lamarche, J., Lewandowski, M., Mansy, J.L., Szulczewski, M., 2003.** Partitioning pre-, syn- and post-Variscan deformation in the Holy Cross Mountains, eastern Variscan foreland. *Geological Society Special Publications*, **208**: 159–184.
- Lamarche, J., Mansy, J.L., Bergerat, F., Averbuch, O., Hakenberg, M., Lewandowski, M., Stupnicka, E., Świdrowska, J., Wajsprych, B., Wieczorek, J., 1999.** Variscan tectonics in the Holy Cross Mountains (Poland) and the role of structural inheritance during Alpine tectonics. *Tectonophysics*, **313**: 171–186.
- Laurent, A., Janousek, V., Magna, T., Schulmann, K., Mikova, J., 2014.** Petrogenesis and geochronology of a postorogenic calc-alkaline magmatic association: the Zuloa Pluton, Bohemian Massif. *Journal of Geosciences*, **59**: 415–440.
- Lewandowska, A., Banaś, M., Zygoń, K., 2007.** K-Ar dating of amphiboles from andesite of complex dyke in Dubie (southern Poland). *Geochronometria*, **27**: 11–15.
- Lewandowski, M., 1999.** Palaeomagnetic study of fracture fills in the Holy Cross Mountains of Central Poland and its application in dating tectonic processes. *Geophysics Journal International*, **317**: 783–792.
- Malec, J., 2001.** Sedimentology of deposits around the Late Caledonian unconformity in the western Holy Cross Mountains. *Geological Quarterly*, **45** (4): 397–415.
- Malec, J., 2006.** Sylur w Górach Świętokrzyskich (in Polish). In: *Procesy i zdarzenia w historii geologicznej Gór Świętokrzyskich* (eds. S. Skompski and A. Żylińska): 36–50. LXXVII Zjazd Naukowy Polskiego Towarzystwa Geologicznego, Ameliówka k. Kielc, 28–30 czerwca 2006 r. Polskie Towarzystwo Geologiczne, Państwowy Instytut Geologiczny, Wydział Geologii Uniwersytetu Warszawskiego.
- Malec, J., Kuleta, M., Migaszewski, Z., 2016.** Lithologic-petrographic characterization of Silurian rocks in the Niestachów profile (Holy Cross Mountains). *Annales Societatis Geologorum Poloniae*, **86**: 85–110.
- Malinowski, M., Żelaźniewicz, A., Grad, M., Guterch, A., Janik, T., 2005.** Seismic and geological structure of the crust in the transition from Baltica to Palaeozoic Europe in SE Poland-CELEBRATION 2000 experiment, profile CEL02. *Tectonophysics*, **401**: 55–77.
- Masiak, M., 2007.** Sylur synkliny bardziańskiej (in Polish). In: *Granice Paleontologii* (ed. A. Żylińska): 149–157. XX Konferencja Naukowa Paleobiologów i Biostratygrafów Polskiego Towarzystwa Geologicznego, Św. Katarzyna pod Łysicą 10–13 września 2007 r., Abstracts and Guide Book, Wydział Geologii Uniwersytetu Warszawskiego.
- Masiak, M., 2010.** Silurian of the Bardo Syncline. In: *Guidebook of the Holy Cross Mountains field trip* (eds. M. Oliwkiewicz-Mikłasińska, A. Łaptaś, W. Trela, M. Stempień-Sałek and M. Masiak): 38–41. CIMP Poland 2010 General Meeting, Warszawa.
- Mattinson, J.M., 1978.** Age, origin, and thermal histories of some plutonic rocks from Salinian Block of California. *Contributions to Mineralogy and Petrology*, **67**: 233–245.
- Mazur, S., Aleksandrowski, P., Kryza, R., Oberc-Dziedzic, T., 2006.** The Variscan Orogen in Poland. *Geological Quarterly*, **50** (1): 89–118.
- Mazur, S., Jarosiński, M., 2006.** Deep basement structure of the Paleozoic platform in SW Poland in the light of POLONAISE-97 seismic experiment (in Polish with English summary). *Prace Państwowego Instytutu Geologicznego*, **188**: 203–222.
- Mazur, S., Mikołajczak, P., Krzywiec, M., Malinowski, V., Buffenmyer, V., Lewandowski, M., 2015.** Is the Teisseyre-Tornquist Zone an ancient plate boundary of Baltica? *Tectonics*, **34**: 2465–2477.
- Mazur, S., Krzywiec, P., Malinowski, M., Lewandowski, M., Aleksandrowski, P., Mikołajczak, M., 2018.** On the nature of the Teisseyre-Tornquist Zone. *Geology, Geophysics and Environment*, **44**: 17–30.
- McDowell, S.D., Elders, W.A., 1980.** Authigenic layer silicate minerals in borehole Elmore I, Salton Sea geothermal field, California, USA. *Contributions to Mineralogy and Petrology*, **74**: 293–310.
- Migaszewski, Z., 2002.** K-Ar and Ar-Ar dating of diabases and lamprophyres from the Holy Cross Mts (central Poland) (in Polish with English summary). *Przegląd Geologiczny*, **50**: 227–229.
- Mitchell, J.G., Taka, A.S., 1984.** Potassium and argon loss patterns in weathered micas: implications for detrital mineral studies, with particular reference to the triassic palaeogeography of the British Isles. *Sedimentary Geology*, **39**: 27–52.
- Mizerski, W., Orłowski, S., Różycki, A., 1986.** Tectonic of the Pasma Ociesęckie and Pasma Zamczyska Ranges in the Góry Świętokrzyskie Mts (in Polish with English summary). *Geological Quarterly*, **30** (2): 187–200.
- Narkiewicz, M., Resak, M., Littke, R., Marynowski, L., 2010.** New constraints on the Middle Palaeozoic to Cenozoic burial and thermal history of the Holy Cross Mts. (central Poland): results from numerical modelling. *Geologica Acta*, **8**: 189–205.
- Narkiewicz, M., Maksym, A., Malinowski, M., Grad, M., Guterch, A., Petecki, Z., Probulski, J., Janik, T., Majdański, M., Środa, P., Czuba, W., Gaczyński, E., Jankowski, L., 2015.** Transcurrent nature of the Teisseyre-Tornquist Zone in Central Europe: results of the POLCRUST-01 deep reflection seismic profile. *International Journal of Earth Sciences*, **104**: 775–796.
- Nawrocki, J., 1999.** Prefolding remanent magnetization of diabase intrusion from the Bardo syncline in the Holy Cross Mts. (Central Poland) (in Polish with English summary). *Przegląd Geologiczny*, **47**: 1101–1104.
- Nawrocki, J., 2000.** Late Silurian paleomagnetic pole from the Holy Cross Mountains: constraints for the post-Caledonian tectonic activity of the Trans-European Suture Zone. *Earth and Planetary Science Letters*, **179**: 325–334.
- Nawrocki, J., Poprawa, P., 2006.** Development of Trans-European Suture Zone in Poland: from Ediacaran rifting to Early Palaeozoic accretion. *Geological Quarterly*, **50** (1): 59–76.
- Nawrocki, J., Dunlap, J., Pecskey, Z., Krzemiński, L., Żylińska, A., Fanning, M., Kozłowski, W., Salwa, S., Szczepanik, Z., Trela, W., 2007.** Late Neoproterozoic to Early Palaeozoic palaeogeography of the Holy Cross Mountains (Central Europe): an integrated approach. *Journal of the Geological Society*, **164**: 405–423.
- Nawrocki, J., Fanning, M., Lewandowska, A., Polechońska, O., Werner, T., 2008.** Palaeomagnetism and the age of the Cracow volcanic rocks (S Poland). *Geophysical Journal International*, **174**: 475–488.
- Nawrocki, J., Krzemiński, L., Pańczyk, M., 2010.** <sup>40</sup>Ar–<sup>39</sup>Ar ages of selected rocks and minerals from the Kraków–Lubliniec Fault Zone, and their relation to the Paleozoic structural evolution of the Małopolska and Brunovistulian terranes (S Poland). *Geological Quarterly*, **54** (3): 289–300.
- Nawrocki, J., Salwa, S., Pańczyk, M., 2013.** New <sup>40</sup>Ar–<sup>39</sup>Ar age constrains for magmatic and hydrothermal activity in the Holy

- Cross Mts. (southern Poland). *Geological Quarterly*, **57** (3): 551–560.
- Nenoen, V., Dick, P., Sammaljärvi, J., Johansson, B., Voutilainen, M., Siitari-Kauppi, M., 2019.** Sealing, healing and fluid flow in clay rocks: insights on episodic flow events in fault zones. Fifth International Conference on Fault and Top Seals 2019, EAGE, Palermo, Italy: 1–5.
- Odin, G.S., Adams, C.J., Armstrong, R.L., Bagdasaryan, G.P., Baksi, A.K., Balogh, K., Barnes, I.L., Boelrijk, N.A.I.M., Bonadonna, F.P., Bonhomme, M.G., Cassagnol, C., Chanin, L., Gillot, P.Y., Geldhill, A., Govindaraju, K., Harakal, R., Harre, W., Hebeda, E.H., Hunziker, J., Ingamells, C.O., Kawashita, K., Kiss, E., Kreuzer, H., Long, L.E., McDougall, I., McDowell, F., Mehnert, H., Montigny, R., Pasteels, P., Radicati, F., Rex, D.C., Rundle, C.C., Savelli, C., Sonet, J., Welin, E., Zimmermann, J.L., 1982.** Interlaboratory Standards for Dating Purposes. In: *Numerical Dating in Stratigraphy* (ed. G.S. Odin): 123–150. John Wiley and Sons.
- O'Hara, K., 2004.** Paleo-stress estimates on ancient seismogenic faults based on frictional heating of coal. *Geophysical Research Letters*, **31**: L03601.
- Oohashi, K., Hirose, T., Takahashi, M., Tanikawa, W., 2015.** Dynamic weakening of smectite-bearing faults at intermediate velocities: implications for subduction zone earthquakes. *Journal of Geophysical Research. Solid Earth*, **120**: 1–15.
- Orłowski, S., Mizerski, W., 1995.** New data on geology of the Middle Cambrian rocks in Klimontów Anticlinorium (Holy Cross Mountains). *Geological Quarterly*, **39** (3): 293–306.
- Pańczyk, M., Nawrocki, J., 2015.** Tournaisian  $^{40}\text{Ar}/^{39}\text{Ar}$  age for alkaline basalts from the Lublin Basin (SE Poland). *Geological Quarterly*, **59** (3): 473–478.
- Pharaoh, T.C., 1999.** Palaeozoic terranes and their lithospheric boundaries within the Trans-European Suture Zone (TESZ): a review. *Tectonophysics*, **314**: 17–41.
- Pharaoh, T., and TESZ colleagues, 1996.** Trans-European Suture Zone: Phanerozoic accretion and the evolution of contrasting continental lithosphere, EUROPROBE 1996 – lithosphere dynamics: origin and evolution of continents. *Europrobe Secretariate*, Uppsala University: 41–54.
- Pharaoh, T.C., Winchester, J.A., Verniers, J., Lasse, A., Seghedi, A., 2006.** The western accretionary margin of the east European craton: an overview. *Geological Society of London Memoir*, **32**: 291–311.
- Pietranik, A., Storey, C., Kierczak, J., 2013.** The Niemcza diorites and monzoniorites (Sudetes, SW Poland): a record of changing geotectonic setting at ca. 340 Ma. *Geological Quarterly*, **57** (2): 325–334.
- Požaryski, W., Grocholski, A., Tomczyk, H., Karnkowski, P., Moryc, W., 1992.** The tectonic map of Poland in the Variscan epoch (in Polish with English summary). *Przegląd Geologiczny*, **40**: 643–650.
- Racki, G., 2006.** Zarys stratygrafii (in Polish). In: *Procesy i zdarzenia w historii geologicznej Gór Świętokrzyskich* (eds. S. Skompski and A. Żylińska): 51–55. LXXVII Zjazd Naukowy Polskiego Towarzystwa Geologicznego, Ameliówka k. Kielc, 28–30 czerwca 2006 r. Polskie Towarzystwo Geologiczne, Państwowy Instytut Geologiczny, Wydział Geologii Uniwersytetu Warszawskiego.
- Reyes, A.G., 1990.** Petrology of Philippine geothermal systems and the application of alteration mineralogy to their assessment. *Journal of Volcanology and Geothermal Research*, **43**: 279–309.
- Rice, J.R., 2006.** Heating and weakening of faults during earthquake slip. *Journal of Geophysical Research*, **111**: B05311, 1–29.
- Rubinowski, Z., 1962.** The lamprophyres of the Daleszyce region (Święty Krzyż Mountains) and mineralization symptoms connected with them (in Polish with English summary). *Geological Quarterly*, **6** (3): 245–269.
- Rutter, E.H., Holdsworth, R.E., Knipe, R.J., 2001.** The nature and tectonic significance of fault zone weakening: an introduction. *Geological Society Special Publications*, **186**: 1–11.
- Samson, S.D., Alexander, E.C. Jr., 1987.** Calibration of the interlaboratory  $^{40}\text{Ar}/^{39}\text{Ar}$  dating standard, Mmh-1. *Chemical Geology (Isotope Geoscience Section)*, **66**: 27–34.
- Samsonowicz, J., 1934.** Explication de la feuille Opatów. *Carte Géologique Générale de la Pologne au 100 000*. Varsovie.
- Schätz, M., Zwing, A., Tait, J., Belka, Z., Soffel, H.C., Bachtadse, V., 2006.** Paleomagnetism of Ordovician carbonate rocks from Malopolska Massif, Holy Cross Mountains, SE Poland – magnetostratigraphic and geotectonic implications. *Earth and Planetary Science Letters*, **244**: 349–360.
- Schleicher, A., Sutherland, R., Townend, J., Toy, V., van der Pluijm, B., 2015.** Clay mineral formation and fabric development in the DFDP-1B borehole, central Alpine Fault, New Zealand. *New Zealand Journal of Geology and Geophysics*, **58**: 1–9.
- Smit, J., van Wees, J.-D., Cloetingh, S., 2016.** The Thor suture zone: from subduction to intraplate basin setting. *Geology*, **44**: 707–710.
- Stesky, R.M., 1978.** Mechanisms of high temperature frictional sliding in Westerly granite. *Canadian Journal of Earth Sciences*, **15**: 361–375.
- Stevens, R.D., Delabio, R.N., Lachance, G.R., 1982.** Age determinations and geological studies K-Ar isotopic ages, Report 15. *Geological Survey of Canada Paper*, **81**: 1–56.
- Stipp, M., Stünitz, H., Heilbronner, R., Schmid, S.M., 2002a.** The eastern Tonale fault zone: a “natural laboratory” for crystal plastic deformation of quartz over a temperature range from 250 to 700°C. *Journal of Structural Geology*, **24**: 1861–1884.
- Stipp, M., Stünitz, H., Heilbronner, R., Schmid, S.M., 2002b.** Dynamic recrystallization of quartz: Correlation between natural and experimental conditions. *Geological Society Special Publications*, **200**: 171–190.
- Stoch, L., Sikora, W., 1976.** Transformations of micas in the process of kaolinitization of granites and gneisses. *Clays and Clay Minerals*, **24**: 156–162.
- Stupnicka, E., 1995.** Fazy ruchów tektonicznych w górnym sylurze i dolnym dewonie w południowej części Gór Świętokrzyskich (in Polish). *Przegląd Geologiczny*, **43**: 110–112.
- Szaniawski, R., 2008.** Late Palaeozoic geodynamics of the Malopolska Massif in the light of new palaeomagnetic data for the southern Holy Cross Mountains. *Acta Geologica Polonica*, **58**: 1–12.
- Szaniawski, R., Konon, A., Grabowski, J., Schnabl, P., 2011.** Paleomagnetic age constraints on folding and faulting events in Devonian carbonates of the Kielce Fold Zone (southern Holy Cross Mountains, Central Poland). *Geological Quarterly*, **55** (3): 223–234.
- Szczepanik, Z., Trela, W., Salwa, S., 2004.** Upper Cambrian in the Kielce Region of the Holy Cross Mts. – preliminary report (in Polish with English summary). *Przegląd Geologiczny*, **52**: 895–898.
- Szulczewski, M., 1995.** Depositional evolution of the Holy Cross Mts. (Poland) in the Devonian and Carboniferous – a review. *Geological Quarterly*, **39** (1): 471–488.
- Šucha, V., Kraus, I., Gerthofferova, H., Petes, J., Serekova, M., 1993.** Smectite to illite conversion in bentonites and shales of the East Slovak Basin. *Clay Minerals*, **28**: 243–253.
- Tomczyk, H., 1962.** Stratigraphic problems of the Ordovician and Silurian in Poland in the light of recent studies (in Polish with English summary). *Prace Instytutu Geologicznego*, **35**.
- Trela, W., 2006.** Ordowik w Górach Świętokrzyskich: zapis stratygraficzny i sedimentacyjny (in Polish). In: *Procesy i zdarzenia w historii geologicznej Gór Świętokrzyskich* (eds. S. Skompski and A. Żylińska): 28–35. LXXVII Zjazd Naukowy Polskiego Towarzystwa Geologicznego, Ameliówka k. Kielc, 28–30 czerwca 2006 r. Polskie Towarzystwo Geologiczne, Państwowy Instytut Geologiczny, Wydział Geologii Uniwersytetu Warszawskiego.
- Turniak, K., Mazur, S., Domańska-Siuda, J., Szuszkiewicz, A., 2014.** SHRIMP U-Pb zircon dating for granitoids from the Strzegom-Sobótka Massif, SW Poland: constraints on the initial time of Permo-Mesozoic lithosphere thinning beneath Central Europe. *Lithos*, **208–209**: 415–429.

- van Daalen, M., Heilbronner, R., Kunze, K., 1999. Orientation analysis of localized shear deformation in quartz fibres at the brittle–ductile transition. *Tectonophysics*, **303**: 83–107.
- Vidal, O., Baldeyrou, A., Beaufort, D., Fritz, B., Geoffroy, N., Lanson, B., 2012. Experimental study of the stability and phase relations of clays at high temperature in a thermal gradient. *Clays and Clay Minerals*, **60**: 200–225.
- Villa, I.M., 2010. Disequilibrium textures versus equilibrium modeling: geochronology at the crossroads. *Geological Society Special Publications*, **332**: 1–15.
- Voll, G., 1976. Recrystallization of quartz, biotite and feldspars from Erstfeld to the Leventina Nappe, Swiss Alps, and its geological significance. *Schweizerische Mineralogische und Petrographische Mitteilungen*, **56**: 641–647.
- Walczak, A., Belka, Z., 2017. Fingerprinting Gondwana versus Baltica provenance: Nd and Sr isotopes in Lower Paleozoic clastic rocks of the Małopolska and Łysogóry terranes, southern Poland. *Gondwana Research*, **45**: 138–151.
- Walczowski, A., 1968. *Objaśnienia do szczegółowej mapy geologicznej Polski 1:50 000, arkusz Łagów* (in Polish). Wyd. Geol., Warszawa.
- Walker, R.J., Holdsworth, R.E., Armitage, P.J., Faulkner, D.R., 2013. Fault zone permeability structure evolution in basalts. *Geology*, **41**: 59–62.
- White, N.C., Hedenquist, J.W., 1995. Epithermal gold deposits: Styles, characteristics and exploration. *Society of Economic Geologists Newsletter*, **23**: 1–9.
- Whitney, C., 1990. Role of water in the smectite-to-illite reaction. *Clays and Clay Minerals*, **38**: 343–350.
- Wójcik, E., 2017. Geochemistry of a newly discovered tuffite from the Ludlow (Silurian) strata of the Bardo Syncline, Holy Cross Mountains, Poland. In: 10th Baltic Stratigraphic Conference (ed. A. Żylińska): 101–107. Chęciny 12–14 September, Abstracts and Guide Book, Warszawa.
- Winchester, J.A., Pharaoh, T.C., Verniers, J., 2002a. Palaeozoic amalgamation of Central Europe: an introduction and synthesis of new results from recent geological and geophysical investigations. *Geological Society Special Publications*, **201**: 1–18.
- Winchester, J.A., the Pace TMR Network Team, 2002b. Palaeozoic amalgamation of Central Europe: new results from recent geological and geophysical investigations. *Tectonophysics*, **360**: 5–21.
- Winchester, J.A., Pharaoh, T.C., Verniers, J., Ioane, D., Seghedi, A., 2006. Palaeozoic accretion of Gondwana-derived terranes to the East European Craton: recognition of detached terrane fragments dispersed after collision with promontories. *Geological Society of London Memoir*, **32**: 323–332.
- Wintsch, R.P., Christoffersen, R., Kronenberg, A.K., 1995. Fluid-rock reaction weakening of fault zones. *Journal of Geophysical Research*, **100**: 13021–13032.
- Yamada, R., Mizoguchi, K., 2011. Thermal anomaly and strength of Atotsugawa fault, central Japan, inferred from fission-track thermochronology. In: *Developments in Heat Transfer* (ed. M.A. Dos Santos Bernardes). InTech.
- Yang, T., Dekkers, M.J., Zhang, B., 2016. Seismic heating signatures in the Japan Trench subduction plate boundary fault zone: Evidence from a preliminary rock magnetic "geothermometer". *Geophysical Journal International*, **205**: 332–344.
- Zwing, A., 2003. Causes and mechanisms of remagnetisation of Palaeozoic sedimentary rocks: a multidisciplinary approach. Ph.D. thesis, LMU München.
- Żelaźniewicz, A., Buła, Z., Fanning, M., Seghedi, A., Żaba, J., 2009. More evidence on Neoproterozoic terranes in southern Poland and southeastern Romania. *Geological Quarterly*, **53** (1): 93–124.
- Żelaźniewicz, A., Oberc-Dziedzic, T., Fanning, C.M., Protas, A., Muszyński, A., 2016. Late Carboniferous–Early Permian events in the Trans–European Suture Zone: tectonic and acid magmatic evidence from Poland. *Tectonophysics*, **675**: 227–243.
- Żylińska, A., 2017. Outline of the Palaeozoic geology of the Holy Cross Mountains. In: 10th Baltic Stratigraphic Conference (ed. A. Żylińska): 101–107. Chęciny 12–14 September, Abstracts and Guide Book, Warszawa.